Approaching the Gas-Phase Structures of $[AgS_8]^+$ and $[AgS_{16}]^+$ in the Solid State

T. Stanley Cameron,[b][1] Andreas Decken,[c][2] Isabelle Dionne,[c][3] Min Fang,[c][3] Ingo Krossing,*[a][4] and Jack Passmore[c][4]

Abstract: Upon treating elemental sulfur with $[AgSbF_6]$, $[AgAl(hfip)_4]$, $[AgAl(pftb)_4]$ (hfip = $OCH(CF_3)_2$, pftb = $OC(CF_3)_3$) the compounds $[Ag(S_8)_2][SbF_6]$ (**1**), $[AgS_8][Al(hfip)_4]$ (**2**), and $[Ag(S_8)_2]^+[[Al(pftb)_4]^-$ (**3**) formed in SO_2 (**1**), CS_2 (**2**), or CH_2Cl_2 (**3**). Compounds **1**–**3** were characterized by single-crystal X-ray structure determinations: **1** by Raman spectroscopy, **2** and **3** by solution NMR spectroscopy and elemental analyses. Single crystals of $[Ag(S_8)_2]^+[Sb(OTeF_5)_6]^-$ **4** were obtained from a disproportionation reaction and only characterized by X-ray crystal structure analysis. The Ag^+ ion in **1** coordinates two monodentate SbF_6^- anions and two bidentate S_8 rings in the 1,3-position. Compound **2** contains an almost C_{4v}-symmetric $\{AgS_8\}^+$ moiety; this is the first example of an η^4-coordinated S_8 ring (d(Ag–S) = 2.84–3.00 Å). Compounds **3** and **4**, with the least basic anions, contain undistorted, approximately centrosymmetric $Ag(\eta^4\text{-}S_8)_2^+$ cations with less symmetric η^4-coordinated S_8 rings (d(Ag–S) = 2.68–3.35 Å). The thermochemical radius and volume of the undistorted $Ag(S_8)_2^+$ cation was deduced as $r_{therm}(Ag(S_8)_2^+) = 3.378 + 0.076/-0.120$ Å and $V_{therm}(Ag(S_8)_2^+) = 417+4/-6$ Å^3. AgS_8^+ and several isomers of the $Ag(S_8)_2^+$ cation were optimized at the BP86, B3LYP, and MP2 levels by using the SVP and TZVPP basis sets. An analysis of the calculated geometries showed the MP2/TZVPP level to give geometries closest to the experimental data. Neither BP86 nor B3LYP reproduced the longer weak dispersive Ag–S interactions in $Ag(\eta^4\text{-}S_8)_2^+$ but led to $Ag(\eta^3\text{-}S_8)_2^+$ geometries. With the most accurate MP2/TZVPP level, the enthalpies of formation of the gaseous $[AgS_8]^+$ and $[Ag(S_8)_2]^+$ cations were established as $\Delta_f H^{298}([Ag(S_8)_2]^+, g) = 856$ kJ mol^{-1} and $\Delta_f H^{298}([AgS_8]^+, g) = 902$ kJ mol^{-1}. It is shown that the $\{AgS_8\}^+$ moiety in **2** and the $\{AgS_8\}_2^+$ cations in **3** and **4** are the best approximation of these ions, which were earlier observed by MS methods. Both cations reside in shallow potential-energy wells where larger structural changes only lead to small increases in the overall energy. It is shown that the covalent Ag–S bonding contributions in both cations may be described by two components: i) the interaction of the spherical empty Ag $5s^0$ acceptor orbital with the filled S $3p^2$ lone-pair donor orbitals and ii) the interaction of the empty Ag $5p^0$ acceptor orbitals with the filled S $3p^2$ lone-pair donor orbitals. This latter contribution is responsible for the observedlow symmetry of the centrosymmetric $Ag(\eta^4\text{-}S_8)_2^+$ cation. The positive charge transferred from the Ag^+ ion in **1**–**4** to the coordinated sulfur atoms is delocalized over all the atoms in the S_8 ring by multiple $3p^2 \rightarrow 3\sigma^*$ interactions that result in a small long-short-long-short S–S bond-length alternation starting from S1 with the shortest Ag–S length. The driving force for all these weak bonding interactions is positive charge delocalization from the formally fully localized charge of the Ag^+ ion.

Keywords: ab initio calculations · cations · density functional theory · silver · sulfur · weakly coordinating anion

Introduction

Many cations and anions that are unknown in condensed phases have already been characterized in the gas phase by one of the advanced mass spectrometric (MS) methods. Recent examples include complexes of P_4 and H^+,[5] Li^+,[6] or Ag^+,[7] as well as those of S_n ($n = 2-8$) and H^+,[8] Ag^+,[9] and 28 other univalent transition metal cations.[9a] However, all MS methods are hampered by the lack of structural information provided by this technique. Quantum chemical investigations of the cations in question tend to be difficult since their potential energy hypersurfaces are flat.[8] Thus, although it has

[a] Dr. I. Krossing[4]
Universität Karlsruhe, Institut für Anorganische Chemie
Engesserstr. Geb. 30.45, 76128 Karlsruhe (Germany)
Fax: (+49) 721-608-48-54
E-mail: krossing@achpc9.chemie.uni-karlsruhe.de

[b] Prof. T. S. Cameron[1]
Chemistry Department, Dalhousie University
Halifax, N.S. (Canada)

[c] A. Decken,[2] MSc. I. Dionne,[3] MSc. M. Fang,[3] Prof. J. Passmore[4]
Chemistry Department, University of New Brunswick
Fredericton, N.B. (Canada)

Supporting information for this article is available on the WWW under http://www.chemeurj.org or from the author.

  0947-6539/02/0815-3386 $ 20.00+.50/0

been established that the $[AgP_4]^+$, $[AgP_8]^+$, $[AgS_4]^+$, $[AgS_8]^+$, and $[AgS_{16}]^+$ cations exist in the gas phase, their geometries remained unknown, with the exception of a distorted $[AgS_{16}]^+$ salt with the $[AsF_6]^-$ anion (see below).[10] However, they may be accessible in the solid state if provided with a very weakly coordinating anion (WCA) such as $[Al(pftb)_4]^-$ (pftb = $OC(CF_3)_3$)[11] or $[Sb(OTeF_5)_6]^-$.[12, 13, 14] In agreement with this, an undistorted homoleptic $[Ag(P_4)_2]^+$ cation formed from $Ag[Al(pftb)_4]$ and P_4,[15] which is presumably the closest approximation to the gaseous $[AgP_8]^+$ cation.[7] We note that the authors of the MS paper[7] postulated a structure with two η^1-bound P_4 molecules. However, the crystal structure of $[Ag(P_4)_2]^+[Al(pftb)_4]^-$ showed the cation to have D_{2h} symmetry, with two coplanar, η^2-coordinated P_4 tetrahedra; this highlights the necessity of an experimental method to establish the geometry of the cation in question. Several binary silver–sulfur complexes—the main objective of this contribution—are known to exist in the gas phase, of which $[AgS_4]^+$ (presumably $[Ag(S_2)_2]^+$), $[AgS_8]^+$ (presumably $[AgS_8]^+$) and $[AgS_{16}]^+$ (presumably $[Ag(S_8)_2]^+$) gave the highest intensities in the MS.[9] In contrast, only two complexes with an intact S_8 crown ring acting as a ligand have been structurally characterized in the solid state,[16] that is, $[S_8Rh_2(O_2CCF_3)_4]$[17] and $[Ag(S_8)_2AsF_6]$.[10] Copper(I) halides were recently shown to interact weakly with the rings and chains of the heavier chalcogens as well as with related phosphorus or mixed phosphorus–selenium cages.[18, 19] The structure of $[Ag(S_8)_2AsF_6]$, although formally containing an $[Ag(S_8)_2]^+$ cation, is strongly influenced by two Ag–F contacts that considerably distort the geometry of the $[Ag(S_8)_2]^+$ cation, see Figure 1.[20]

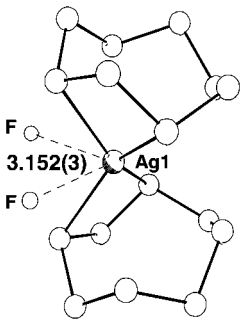

Figure 1. The solid state structure of the $\{Ag(S_8)_2\}$ moiety in $[Ag(S_8)_2][AsF_6]$[10] including the two Ag–F contacts.[20]

Consequently, $[AsF_6]^-$ is too basic to provide an environment for the free and undistorted $[AgS_{16}]^+$ or $[AgS_8]^+$ cations, and their geometries remain unknown. The undistorted $[Ag(S_8)_2]^+$ ion in $[Ag(S_8)_2]^+[Sb(OTeF_5)_6^-]$ was initially prepared by us as one of the products of a complex reaction. An X-ray structure was obtained but the standard deviations of the structural parameters were high. The reaction of Ag[Al(hfip)$_4$] and Ag[Al(pftb)$_4$] (hfip = $OCH(CF_3)_2$, pftb = $OC(CF_3)_3$) with S_8 resulted quantitatively in the formation of salts of an almost undistorted $[AgS_8]^+$ (as shown by X-ray) as well as a truly undistorted $[Ag(S_8)_2]^+$ cation (X-ray). We also include the preparation and X-ray crystal structure of $[Ag(S_8)_2][SbF_6]$. The structure and bonding of these silver–sulfur cations was thoroughly examined based on the experimental results and the quantum chemical calculations.

Results and Discussion

Syntheses: $[Ag(S_8)_2][SbF_6]$ (**1**) was prepared by a modification of the reported method,[10b] by using $[AgSbF_6]$ instead of $[AgAsF_6]$ and treating it with S_8 in SO_2 solution according to Equation (1):

$$[AgSbF_6] + 2S_8 \longrightarrow [Ag(S_8)_2][SbF_6] \quad (1)$$

This procedure yielded microcrystalline powders of **1** in quantitative yield, which were identified by Raman spectroscopy. Single crystals were obtained from a disproportionation reaction (see Supporting Information for details). The solid-state structure of **1** with two $[SbF_6]^-$ anions coordinated to the silver cation is isostructural to the known $[Ag(S_8)_2][AsF_6]$.[10] Therefore we changed this classical anion to the larger $Al(OR)_4^-$ type anions. When S_8 and AgAl(hfip)$_4$[11] were allowed to react in pentane or CS_2, a colorless solution formed from which the molecular compound $[AgS_8][Al(hfip)_4]$ (**2**) crystallized in almost quantitative yield as large colorless blocks of up to $10 \times 10 \times 5$ mm [Eq. (2)]:

$$Ag[Al(hfip)_4] + S_8 \longrightarrow [AgS_8][Al(hfip)_4] \quad (2)$$

The high solubility of **2** in nonpolar CS_2 and pentane suggested that this compound retains its molecular solid state structure—with a coordinated $[Al(hfip)_4]^-$ anion (see below)—also in solution. On replacing $[Al(hfip)_4]^-$ by the less basic $[Al(pftb)_4]^-$ anion, the Ag^+ ion binds two molecules of S_8 giving the $[Ag(S_8)_2]^+[Al(pftb)_4]^-$ salt **3**, which is highly soluble in CH_2Cl_2, in almost quantitative yield [Eq. (3)]:

$$Ag[Al(pftb)_4] + 2S_8 \longrightarrow [Ag(S_8)_2]^+[Al(pftb)_4]^- \quad (3)$$

Only **3** crystallized from solutions of $[AgAl(pftb)_4] + nS_8$ ($n = 0.5$, 1.0, and 2.0) in CH_2Cl_2 with the conditions employed. Therefore it is more favorable for the $\{AgS_8\}^+$ moiety in **3** to interact with a second molecule of S_8 than with the $[Al(pftb)_4]^-$ anion, and the neutral S_8 molecule is more basic toward the silver ion than the $[Al(pftb)_4]^-$ anion. This may be contrasted with the coordination of the more basic $[Al(hfip)_4]^-$ anion in **2**. Similarly the crystal structure of $[AgP_4][Al(hfip)_4]$ contains a coordinated anion while $[Ag(P_4)_2]^+[Al(pftb)_4]^-$, with the less basic anion, is a salt.[15] Solid and dissolved **2** and **3** are very sensitive toward atmospheric conditions and turn brownish-black within less than a second when exposed to air. Several attempts to obtain room temperature Raman spectra of **2** and **3** failed, even with low laser energy (25 mW) and a wide focus, due to decomposition evidenced by the dark appearance of the sample after the acquisition of the Raman data (1064 nm radiation).[21]

The undistorted $[Ag(S_8)_2]^+$ cation was first obtained with the large $[Sb(OTeF_5)_6]^-$ anion: $[Ag(S_8)_2]^+[Sb(OTeF_5)_6]^-$ (**4**), colorless single crystals of which formed as a by-product of the reaction between sulfur, bromine and $Ag[Sb(OTeF_5)_6]$[13, 22] and subsequent recrystallization from SO_2ClF—possibly as in Equation (4) (not balanced):

$$2.44\,S + 1.44\,Br + Ag[Sb(OTeF_5)_6] \xrightarrow{SO_2,\ 20\,^\circ C} [Ag(S_8)_2]^+[Sb(OTeF_5)_6^-]\ (+\ [SBr_3][Sb(OTeF_5)_6] + AgBr + \ldots?) \quad (4)$$

Compound **4** was only characterized by its solid state structure.

  0947-6539/02/0815-3387 $ 20.00+.50/0

Crystal structures: Details on structure solution and refinement are included in Table 9 below. A discussion of the overall structures of **1**–**4**, the solid state packing of the salts **3** and **4**, and the geometries of the anions is included in the Supporting Information. The anion in **3** undergoes a substantial ordering process between 150 and 200 K: at 150 K the $[Al(pftb)_4]^-$ anion is ordered, and the $[Ag(S_8)_2]^+$ cation has C_1 symmetry with three primary Ag–S contacts at 2.622(2), 2.794(2), and 2.838(2) Å. At 200 K, the slightly disordered anion has large displacement parameters indicative of free rotation of the CF_3 groups around the C–C bond, and the (ordered) cation is almost centrosymmetric with considerably rearranged coordination of the S_8 rings as evidenced from the four primary Ag–S contacts at 2.691(5), 2.708(5), 2.921(5), and 2.937(5) Å. A similar anion ordering phenomenon between 150 and 200 K was observed in $[Ag(P_4)_2]^+$-$[Al(pftb)_4^-]$.[15]

The $\{AgS_8\}^+$ and $\{Ag(S_8)_2\}^+$ moieties: The geometries, solid state contacts, and bond valences s[25] of all the $[AgS_8]^+$ and $[Ag(S_8)_2]^+$ units are compared in Table 1 below. The structural parameters of the individual $\{Ag(S_8)_x\}$ ($x = 1,2$) moieties are included in Figures 2 and 3.

The Ag atom of the C_2-symmetric $[Ag(S_8)_2]^+$ cation in $[Ag(S_8)_2][MF_6]$ is pseudo tetrahedrally surrounded by four Ag–S contacts at 2.774(3) (2×) and 2.802(3) Å (2×) (M = As) or 2.744(1) (2×) and 2.792(1) Å (2×) (M = Sb). Both rings coordinate in a 1,3-bidentate fashion to the Ag^+ ion and the other Ag–S contacts, at 3.420(3) (2×) and 3.471(3) Å (2×) (M = As) or 3.461(1) (2×) and 3.472(3) Å (2×) (M = Sb), are very weak. Silver coordination is completed by two Ag–F contacts at 3.152(3) (M = As) or 3.016(2) Å (M = Sb) that finally lead to a distorted trigonal prismatic AgS_4F_2 coordination.

In **2** the silver ion binds η^4 to a 1,3,5,7-tetradentate S_8 molecule and the $[Al(hfip)_4]^-$ anion. The $\{Ag(\eta^4\text{-}S_8)\}^+$ moiety in **2** is close to C_{4v} symmetry (Figure 3) with four similar Ag–S bond lengths at 2.835(1)–3.002(1) Å (average: 2.924 Å). This is the first observation of such a tetradentate S_8 ligand. The Ag coordination environment is completed by two oxygen and two fluorine atoms of the anion at d(Ag–O) = 2.345(3) and 2.737(3) Å and d(Ag–F) = 3.230(3) and 3.257(3) Å (Figure 2).

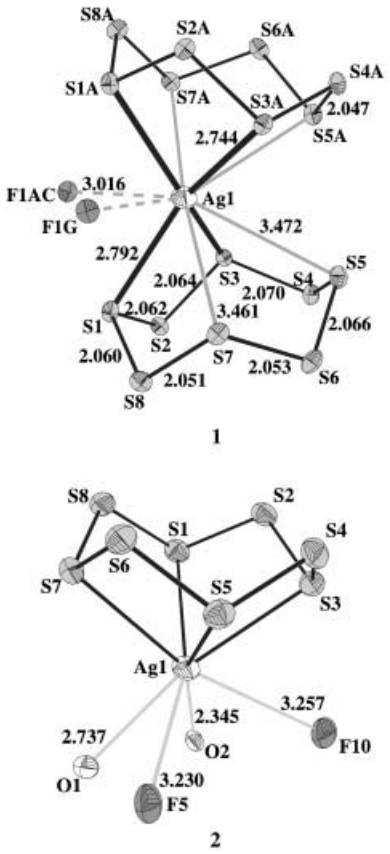

Figure 2. Solid-state structures with coordinated anions: the C_2 symmetric $\{Ag(S_8)_2\}$ moiety in **1**, including the coordinated fluorine atoms, and the AgS_8 unit in **2**, including the coordinated oxygen and fluorine atoms. Bond lengths are given in Å. Sulfur atoms are shown in light gray, silver and oxygen atoms in white, fluorine atoms in dark gray. Anisotropic thermal ellipsoids were drawn at the 25% probability level. Standard deviations (in Å) are: Ag–S = 0.001, S–S = 0.002, Ag–F = 0.002 (**1**) and Ag–O = 0.003, Ag–F = 0.004 (**2**) Å. The structural data of the AgS_8 unit in **2** is included in Figure 3. The black Ag–S bonds are those below 3.0 Å and those shown in gray are the weaker secondary bonds (Table 1).

Table 1. Comparison of the structural parameters and the strengths of the Ag–X and S–F contacts s (X = S, O, F) of the silver–octasulfur complexes in **1**–**4** and $[Ag(S_8)_2][AsF_6]$.[10]

Parameter	$[Ag(S_8)_2][AsF_6]$	**1**	**2**	**3** (150 K)	**3** (200 K)	**4**
d(Ag–S) [Å], s [v.u.]	2.724, 0.209 (2×)	2.744, 0.201 (2×)	2.835, 0.166	2.622, 0.261	2.691, 0.225	2.68, 0.230 (2×)
	2.802, 0.178 (2×)	2.792, 0.181 (2×)	2.912, 0.142	2.794, 0.181	2.708, 0.216	2.99, 0.122 (2×)
	3.420, 0.056 (2×)	3.461, 0.052 (2×)	2.945, 0.133	2.838, 0.165	2.921, 0.140	3.20, 0.082 (2×)
	3.471, 0.051 (2×)	3.472, 0.051 (2×)	3.002, 0.119	3.053, 0.108	2.937, 0.135	3.31, 0.068 (2×)
Also Ag–O			O: 2.345, 0.251	3.173, 0.086	3.159, 0.089	
Also Ag–O			O: 2.737, 0.080	3.182, 0.085	3.199, 0.082	
Also Ag–F	F: 3.152, 0.044	F: 3.016, 0.059	F: 3.230, 0.038	3.271, 0.072	3.330, 0.065	
Also Ag–F	F: 3.152, 0.044	F: 3.016, 0.059	F: 3.257, 0.036	3.524, 0.047	3.354, 0.063	
Σs(Ag–X) [v.u.]	1.076[b]	1.088[c]	0.965[a]	1.005	1.015	1.003
d(S–S)$_{av}$ [Å]	2.050	2.053	2.048	2.050	2.033	2.04
d(S–S)$_{range}$ [Å]	2.041–2.057(3)	2.047–2.070(2)	2.043–2.052(2)	2.038–2.067(3)	2.008–2.048(8)	2.01–2.06(2)
S-S$_{Ag}$-S [°]	107.9–109.3	107.7–109.1	109.0–109.3	108.1–110.0	108.2–109.5	109.5–110.2
S$_{Ag}$-S-S$_{Ag}$ [°]	103.8–107.3	104.1–107.5	104.9–105.8	105.5–107.1	106.0–106.7	105.8–107.5
#(S–F) contacts	14	14	10	18	18	18
d(S–F)$_{range}$	3.051–3.380	3.015–3.347	3.147–3.348	3.011–3.315	3.148–3.399	3.168–3.411
Σs(S–F) [v.u.]	0.861	0.922	0.602	1.035	1.050	1.037

[a] 0.560 (S) + 0.332 (O) + 0.073 (F). [b] 0.988 (S) + 0.088 (F). [c] 0.970 (S) + 0.118 (F).

0947-6539/02/0815-3388 $ 20.00+.50/0 *Chem. Eur. J.* **2002**, *8*, No. 15

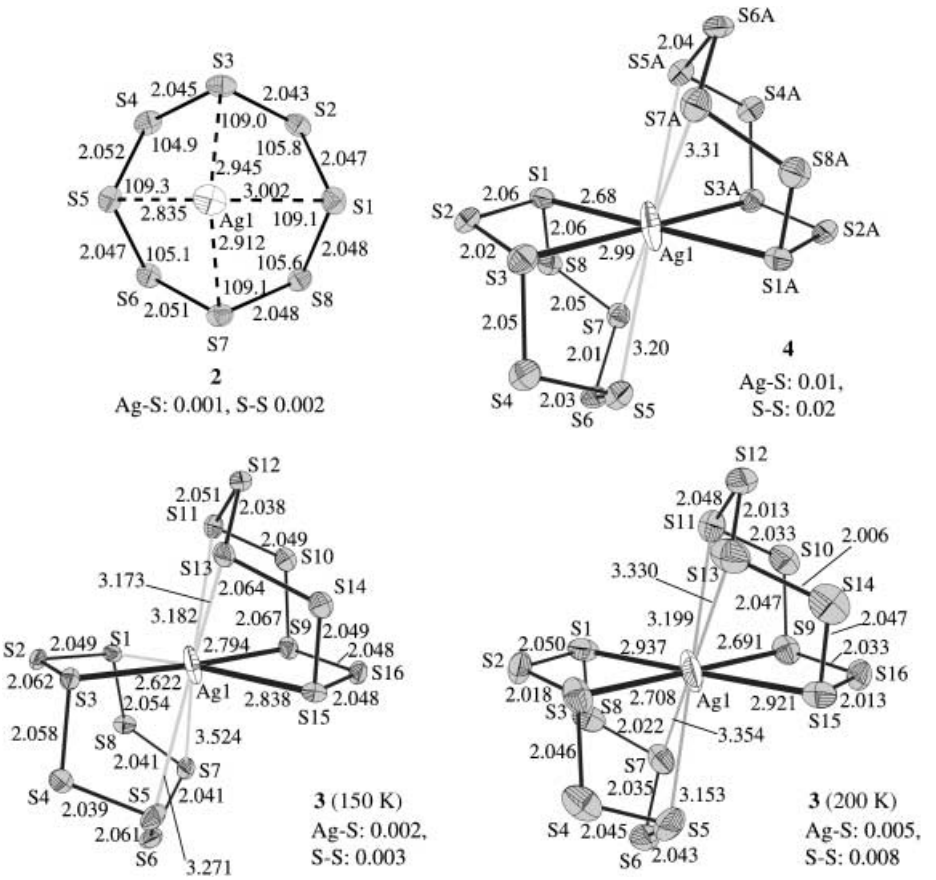

Figure 3. The approximately C_{4v}-symmetric $\{AgS_8\}$ moiety in **2**, the $[Ag(S_8)_2]^+$ cation in **3** at 150 and 200 K, as well as **4**. The cation in **3** (200 K) is almost centrosymmetric and that in **4** is crystallographically centrosymmetric. Bond lengths are given in Å and S-S-S bond angles in degrees, standard deviations in Å are given within the figure. Sulfur atoms are shown in gray and silver atoms in white, anisotropic thermal ellipsoids were drawn at the 25% probability level. The bold black Ag–S bonds are those below 3.0 Å and those shown in gray are the weaker secondary bonds (see Table 1 for details).

To a first order of approximation the $Ag(\eta^4\text{-}S_8)_2^+$ cations in **3**–**4** are sandwich complexes in which the tetradentate S_8 donor molecules fully incorporate the Ag^+ acceptor so that no Ag–F contacts below 4 Å are formed. Closer examination reveals the presence of two different geometries: the unsymmetrical $[Ag(S_8)_2]^+$ structure in **3** (150 K) and the very similar centro- or almost centrosymmetrical structures of the $Ag(\eta^4\text{-}S_8)_2^+$ cation in **3** (200 K) and **4** (see Figure 3). In this last geometry, the silver ion may be described as linear dicoordinate by two stronger Ag–S bonds at 2.700(5) Å (average: **3**, 200 K) or 2.68(1) Å (**4**). The six other weaker contacts range from 2.921(5) to 3.354(5) Å (**3**, 200 K) or from 2.99(1) to 3.31(1) Å (**4**). Alternatively, the primary Ag–S coordination below 3.0 Å can be described as being perfectly planar (see Figure 3). The second $[Ag(S_8)_2]^+$ geometry observed was found in **3** (150 K). It is less regular and may be constructed from one $\{AgS_8\}$ moiety with a similar bonding as in $Ag(S_8)_2MF_6$ (M = As, Sb) and with two shorter Ag–S bond lengths at 2.794(2) and 2.838(2) Å. The bonding of the second S_8 ring in **3** (150 K) is closer to the situation in **4** with one strong Ag–S bond at 2.622(2) Å but all other contacts between 3.053(2) and 3.524(2) Å. The observation of two different $[Ag(S_8)_2]^+$ cations in the solid state structure of **3** at 150 and 200 K indicates that the energetic differences between both cations are minimal although their structural parameters differ considerably (cf. Figure 3).

The S–S bond lengths within all AgS_8 units in Table 1 range from 2.008(8) to 2.070(2) Å, the average of all distances being 2.045 Å. Two distinct sets of S-S-S bond angles are formed: those including a tricoordinate sulfur atom S_{Ag} in the center are wider and range from $S\text{–}S_{Ag}\text{–}S = 107.7 - 110.2^\circ$; those with a dicoordinate sulfur atom are more acute, that is, $S_{Ag}\text{-}S\text{-}S_{Ag} = 103.8 - 107.5^\circ$. Overall the S–S bond lengths and S-S-S bond angles in Table 1 are not significantly different from those of orthorhombic sulfur:[23] $d(S\text{–}S)_{av} = 2.0505(7)$ Å, $d(S\text{–}S)_{range} = 2.0464(8) - 2.0537(6)$ Å, $(S\text{-}S\text{-}S)_{av} = 108.15(2)^\circ$, $(S\text{-}S\text{-}S)_{range} = 107.30(2) - 108.98(2)^\circ$.

All of the coordinated and most of the noncoordinated sulfur atoms exhibit weak S–F contacts to the anions that range from 3.011 to 3.411 Å, the latter is about the sum of the S and F van der Waals radii of 3.30 Å.[24] The number of contacts is related to the basicity of the anions: the less basic the anion, the higher is the number of secondary S–F contacts, that is, there are 14 contacts in $[Ag(S_8)_2][MF_6]$ and 18 in **3** and **4**. Since noncoordinated sulfur atoms also form contacts to fluorine atoms, some charge delocalization from the tricoordinate to the dicoordinate sulfur atoms must have occurred. As Ag^+ and $[Ag(S_8)_2]^+$ are univalent cations, the total of the bond valences *s* of all contacts around the cations below the sum of the respective van der Waals radii is expected to be 1 (usually within 5%, see Supporting Information for details).[25] Both, the sum of the intracationic Ag–S contacts and the interionic S–F contacts in the truly ionic salts **3** and **4** with no Ag–F contacts, give values close to unity (1.003 to 1.050 v.u., Table 1) indicating the validity of the empirical Bond-Valence Method.[25] In $[Ag(S_8)_2][MF_6]$ with two Ag–F contacts, the sum of the S–F bond valences only gives 0.861 (M = As) or 0.922 (M = Sb) v.u.; this shows the structural importance of the Ag–F contacts (As: 0.088, Sb: 0.118 v.u.). In **2** incorporating a coordinated anion, the sum of the bond valences around Ag only reaches unity when contacts to S, O, and F are included. The sum of the Ag–S bond valences to the S_8 molecule in **2** is higher (Ag–S: 0.560 v.u.) than those to the anion (Ag–O: 0.332 v.u., Ag–F: 0.073 v.u.); this underlines the weaker coordination of the Ag^+ cation to the $[Al(hfip)_4]^-$ anion than to S_8. Therefore, the AgS_8 unit in **2** may be an approximation of the gaseous $[AgS_8]^+$ cation (see below).[9] The intramolecular charge transfer from Ag to S of 0.560 v.u. is also reflected in the intermolecular S–F contacts that add up to a similar value of 0.602 v.u. (**2** in Table 1).

Thermochemical radii and volumes of the $[Ag(S_8)_2]^+$ cation: The thermochemical radii and volumes of the $[Al(pftb)_4]^-$ ($r = 4.725$ Å, $V = 758$ Å^3)[26] and $[Sb(OTeF_5)_6]^-$ ($r = 4.79$ Å, $V = 724$ Å^3) anions are known[14]. Therefore the average values for the $[Ag(S_8)_2]^+$ cation can be deduced as:[27]

$$r_{therm}([Ag(S_8)_2]^+) = 3.378 + 0.076/-0.120 \text{ Å}$$

$$V_{therm}([Ag(S_8)_2]^+) = 417 + 4/-6 \text{ Å}^3$$

The lattice potential energies[28] of **3** and **4** can be more reliably established by using thermochemical volumes and are 326 (**3**, 200 K) to 328 (**4**) kJ mol^{-1}. These data may be used as input in further Born–Fajans–Haber cycle calculations, see references [29, 30] and below for examples.

Computational chemistry: To analyze the structure, bonding, and thermochemistry of the gaseous $[Ag(S_8)_n]^+$ ($n = 1, 2$) cations, we optimized the geometries of $[Ag(S_8)_2]^+$, $[AgS_8]^+$, and S_8 (D_{4d}) at the BP86, B3LYP, and (RI-)MP2 level using the double-zeta-quality SVP or triple-zeta-quality TZVPP basis sets. Only the values calculated with the larger and more reliable TZVPP basis set are given. For comparison, the D_{4d}-symmetric neutral S_8 was also calculated (Table 2). Optimizations of gaseous $[AgS_8]^+$ started from the AgS_8^+ geometry in **2** as well as from one half of the $[Ag(S_8)_2]^+$ cation in **4** (C_1 symmetry) but all levels always led to a minimum of approximate C_{4v} symmetry. The final optimizations were done by using this symmetry restraint (Table 2 and Figure 5 below).

The experimental and DFT-calculated S_8 geometries are in good agreement with experiment, and show the usual 0.03–0.05 Å overestimation of the S–S bond length.[31] The ab initio MP2 optimization gave structural data closest to experiment (S–S 0.0075 Å larger than experiment). The S–S bond lengths and S-S-S bond angles of the $[AgS_8]^+$ unit in **2** and the geometries of the calculated C_{4v} $[AgS_8]^+$ cations are in good qualitative agreement (Table 2).

Optimizations of the $[Ag(S_8)_2]^+$ cation started without symmetry by using the nonsymmetric orientation of the cation in **3** at 150 K as well as in C_i symmetry by using the geometry of the centrosymmetric cation in **4** as an input. However, due to the size of the calculation, the MP2/TZVPP optimization of the $[Ag(S_8)_2]^+$ cation was only done in C_i symmetry (see Table 3 for C_i geometries and energies).

Table 3. Optimized geometries of C_i $[Ag(S_8)_2]^+$. Comparison to orthorhombic S_8,[23] the $[Ag(S_8)_2]^+$ cation in **3** (200 K), and the average S–S bond lengths as deduced in Figure 8 (= S–S_{av}).

Parameter [Å]	**3** (200 K)	S–S_{av}	BP86/ TZVPP	B3LYP/ TZVPP	MP2/ TZVPP
Ag1–S1	2.700(5)	–	2.539	2.593	2.609
Ag1–S3	2.929(5)	–	3.225	3.316	2.989
Ag1–S5	3.179(5)	–	3.281	3.321	2.994
Ag1–S7	3.342(5)	–	3.842	3.906	3.408
S1–S2	2.026(8)	2.047	2.117	2.108	2.069
S2–S3	2.032(8)	2.043	2.079	2.077	2.057
S3–S4	2.041(8)	2.048	2.096	2.091	2.062
S4–S5	2.014(8)	2.035	2.086	2.083	2.054
S5–S6	2.024(8)	2.037	2.086	2.083	2.054
S6–S7	2.046(8)	2.048	2.096	2.091	2.062
S7–S8	2.039(8)	2.045	2.079	2.077	2.057
S8–S1	2.047(8)	2.056	2.117	2.108	2.069
S–S (S_8)	2.0505(7)	–	2.092	2.087	2.058

The BP86 and B3LYP C_i optimizations led to geometries close to C_{2h} symmetry, and the silver coordination in the obtained stationary points differs considerably from the geometry observed in the solid state in **3** (200 K) or **4**. This shows strongly in the longest Ag–S contacts, which were weakly bound in the experimental centrosymmetric Ag(η^4-S_8)$_2^+$ at 3.31–3.35 Å, but are nonbonded in the optimized geometries (BP86: 3.84 Å, B3LYP: 3.91 Å; see Table 3), that is, the calculations led to Ag(η^3-S_8)$_2^+$ minima. Also the C_i geometry optimized by MP2 has almost C_{2h} symmetry; however, this calculation led to an Ag(η^4-S_8)$_2^+$ minimum with structural parameters much closer to the experimental data. All calculations gave a small long-short-long-short S–S bond-length alternation starting from S1 with the shortest Ag–S separation (Table 3); this reproduced the experimental results (Figure 8 below). In contrast to the optimization using C_i symmetry, the minimum geometry of the nonsymmetric $[Ag(S_8)_2]^+$ at the BP86/SVP level has an almost D_{4d}-symmetric structure, with a stacked parallel arrangement of the two S_8 rings that was 3.98 kJ mol^{-1} more favorable than the $[Ag(S_8)_2]^+$ geometry optimized in C_i symmetry (Figure 4a).

An MP2/SVP optimization without symmetry also led to this D_{4d} minimum (not shown), while the nonsymmetric B3LYP optimization with the larger and more flexible TZVPP basis set led to a minimum of approximate C_{2h} symmetry, such as the one included in Table 3 or Figure 4b. The existence of C_{2h} and D_{4d} $[Ag(S_8)_2]^+$ geometries, as in Figure 4, therefore appeared likely, and the cations were also optimized with

Table 2. Optimized geometries and total energies of Ag^+, S_8 (D_{4d}), and $[AgS_8]^+$ (C_{4v}). Comparison to orthorhombic S_8[23] and the $\{AgS_8\}^+$ moiety in **2**.

Species	Param.	Exp.	BP86/TZVPP	B3LYP/TZVPP	MP2/TZVPP
Ag^+	E_{tot} [a.u.]	–	– 146.75986	– 146.63335	– 146.21688
S_8[c]	E_{tot} [a.u.]	–	– 3186.11668	– 3185.32542	– 3181.72527
	S–S [Å]	2.0505(7)[a]	2.092	2.087	2.058
	S–S–S [°]	108.15(2)[a]	109.0	108.5	107.4
$[AgS_8]^+$[d]	E_{tot} [a.u.]	–	– 3332.97063	– 3332.03805	– 3328.02537
	Ag–S [Å]	2.835–3.002(1)[b]	2.790	2.860	2.728
	S-S [Å]	2.043–2.051(2)[b]	2.100	2.094	2.066
	S-S_{Ag}-S [°]	109.0–109.3[b]	112.7	111.3	110.1
	S_{Ag}-S-S_{Ag} [°]	104.9–105.8[b]	105.5	105.9	104.4

[a] Orthorhombic S_8.[23] [b] The $\{AgS_8\}^+$ moiety in **2.** [c] ZPE(BP86/SVP): 0.01103 a.u. [d] ZPE(BP86/SVP): 0.01145 a.u.

0947-6539/02/0815-3390 $ 20.00+.50/0 *Chem. Eur. J.* **2002**, *8*, No. 15

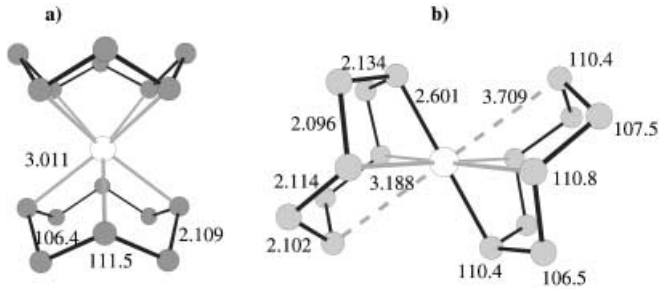

Figure 4. a) BP86/SVP-optimized geometry of C_1 $[Ag(S_8)_2]^+$ with a minimum close to D_{4d} symmetry. The optimization started from the unsymmetrical orientation of the $[Ag(S_8)_2]^+$ cation in the solid state structure of **3** (150 K). b) BP86/SVP-optimized geometry of C_{2h} $[Ag(S_8)_2]^+$.

these symmetries. Their total and relative energies are collected in Table 4, the structural parameters are given in Table 5.

Table 4. Total and relative energies of C_i, C_{2h}, and D_{4d} $Ag(S_8)_2^+$ at the BP86, B3LYP, and (RI-)MP2 levels. Relative energies [kJ mol^{-1}] were obtained including the zero point energy (= ZPE) calculated at the BP86/SVP level.[a]

E_{tot} [a.u.]	BP86/TZVPP	E_{rel}	B3LYP/TZVPP	E_{rel}	MP2/TZVPP	E_{rel}
C_i $[Ag(S_8)_2]^+$	−6519.12226	0	−6517.39565	0	−6509.80022	+17.22
C_{2h} $[Ag(S_8)_2]^+$	−6519.12224	+0.74	−6517.39540	+0.74	−6509.80032	+16.86
D_{4d} $[Ag(S_8)_2]^+$	−6519.12142	+3.35	−6517.39438	+3.33	−6509.80674	0

[a] The BP86/SVP ZPEs are: 0.02275 (C_i), 0.02278 (C_{2h}), 0.02276 (D_{4d}).

Table 5. Optimized geometries of C_{2h} and D_{4d} $[Ag(S_8)_2]^+$. Labeling as in Figure 8.

Species	Param. [Å]	BP86/TZVPP	B3LYP/TZVPP	MP2/TZVPP
C_{2h}	Ag1 – S1	2.546	2.593	2.572
	Ag1–S3	3.245 (4×)	3.325 (4×)	3.016 (4×)
	Ag1–S5	3.830	3.920	3.420
	S1–S2	2.117	2.107	2.071
	S2–S3	2.079	2.077	2.056
	S3–S4	2.096	2.091	2.061
	S4–S5	2.086	2.082	2.055
D_{4d}	Ag–S	3.025	3.091	2.885
	S–S	2.092	2.088	2.061

The small energetic differences between the D_{4d}, C_{2h}, and C_i isomers of only 0.74 – 17.22 kJ mol^{-1} indicate the presence of a very shallow potential energy surface where small energetic changes may lead to drastically changed geometries, that is, although C_i and D_{4d} $Ag(S_8)_2^+$ are almost isoenergetic, their Ag–S distances differ by up to 0.7 – 0.8 Å (cf. Tables 4 and 7 below). From the data in Table 4, the global minimum of the gaseous $[Ag(S_8)_2]^+$ cation cannot be deduced. It might either be D_{4d} symmetric or C_i symmetric. In the BP86 and B3LYP C_i geometries, the primary Ag–S bonds are too short, and all secondary weak bonds are too long if compared with the experimental structure in **3** (200 K) and **4**. Only at the MP2/TZVPP level were the lengths of the secondary Ag–S bonds similar to experiment, although MP2 is not able to reproduce the unsymmetrical silver environment of the experimental cation and gives an almost C_{2h}-symmetric minimum.

Thermodynamics: To establish the quality of the calculations, we assessed the ligand-exchange reaction of the $[Ag(P_4)_2]^+$ cation with S_8 as in Equation (5) (Table 6), which was shown experimentally[15b, 32] to be endergonic in CH_2Cl_2.

$$[Ag(P_4)_2]^+ + 2S_8 \longrightarrow [Ag(S_8)_2]^+ + 2P_4 \quad (5)$$

Table 6. The free energies of a reaction according to Equation (5), solvation energies in CH_2Cl_2 were calculated with the COSMO solvation model.[73] These reflect the experimental findings.

	BP86/SVP	B3LYP/TZVPP	MP2/TZVPP
$\Delta G_{(g)}$[a]	33	57	21
$\Delta G(CH_2Cl_2)$[b]	62	86	50

[a] $\Delta H_{(g)}$ ($\Delta G_{(g)}$) denote the enthalpy (free energy) change in the gas phase at 298 K. [b] Values indexed with (CH_2Cl_2) approximate the solution behavior in CH_2Cl_2 [kJ mol^{-1}].

In agreement with the experimental observation, the calculations showed that the reaction is endergonic in the gas phase and in solution. Therefore we are confident that the computations provide useful insights into the thermodynamics of the system. The energetics of the formation of the gaseous (g) and dissolved (CH_2Cl_2) $[AgS_8]^+$ and $[Ag(S_8)_2]^+$ cations are collected in Table 7.

Table 7. Enthalpies of the reactions of Ag^+ and one or two molecules of S_8.

Reaction	Property	BP86[a]	B3LYP[a]	MP2[a]
(a) $Ag^+ + 2S_8 \rightarrow [Ag(S_8)_2]^+$	$\Delta H_{(g)}$	−334	−290	−363
	$\Delta G_{(g)}$	−256	−210	−283
	$\Delta G(CH_2Cl_2)$	−123	−77	−149
(b) $Ag^+ + S_8 \rightarrow [AgS_8]^+$	$\Delta H_{(g)}$	−245	−206	−216
	$\Delta G_{(g)}$	−212	−173	−184
	$\Delta G(CH_2Cl_2)$	−115	−77	−87
(c) $[AgS_8]^+ + S_8 \rightarrow [Ag(S_8)_2]^+$	$\Delta H_{(g)}$	−91	−84	−147
	$\Delta G_{(g)}$	−44	−37	−100
	$\Delta G(CH_2Cl_2)$	−7	+4	−62

[a] TZVPP basis set.

These reaction enthalpies, obtained by the three different methods, are comparable and differ by a maximum of 73 kJ mol^{-1} [Eq. (a)]. The formation of $[Ag(S_8)_2]^+$ in Equation (a) is also highly exergonic in CH_2Cl_2. The binding of the first S_8 molecule in Equation (b) is more favorable than that of the second S_8 molecule in Equation (c), but according to the BP86 and MP2 values also possible in CH_2Cl_2—the solvent used for the synthesis of **3**. However, exchange reactions of the second S_8 molecule bonded to the silver atom with the solvent will certainly occur in solution. Photodissociation experiments of the gaseous $[AgS_{16}]^+$ cation (193 nm Laser)[9b] indicated that fragmentation with the separation of one S_8 molecule was easily achieved, while the second S_8 molecule could only be released with a much lower photodissociation percentage.[9b] The reaction enthalpies in Table 7 are in good agreement with those observed or calculated for related systems $Ag^+ + 2L \rightarrow [Ag(L)_2]^+$, that is, the $\Delta H_{(g)}$ ($\Delta G_{(g)}$) for $L = C_2H_4$[33] or P_4[15b] is −276.5 (−169.5) or −265 (−186) kJ mol^{-1} (cf. Equation (a) in Table 7). For the reaction $[AgL]^+ + L \rightarrow [Ag(L)_2]^+$: $\Delta H_{(g)}$ ($\Delta G_{(g)}$) for $L = C_2H_4$ or P_4 is

-135.5 (-71.5) or -112 (-61) kJ mol^{-1} (cf. Equation (c) in Table 7).

With our most accurate MP2/TZVPP enthalpy values (see below) and the known heats of formation of Ag^+ (1017 kJ mol^{-1}) and S_8 (101 kJ mol^{-1}), the gaseous enthalpies of formation of $[AgS_8]^+$ and $[Ag(S_8)_2]^+$ are established as:[34]

$$\Delta_f H^{298}([Ag(S_8)_2]^+, g) = 856 \text{ kJ mol}^{-1}$$

$$\Delta_f H^{298}([AgS_8]^+, g) = 902 \text{ kJ mol}^{-1}$$

By using the lattice potential energies estimated from the thermochemical volumes, the experimental sublimation enthalpy of S_8 (101 kJ mol^{-1}),[53] the MP2-calculated gas phase contributions, and a Born–Haber cycle as in Scheme 2 (below), the solid state enthalpy of reaction of $Ag^+[Al(pftb)_4]^-_{(s)}$ with two molecules of $S_{8(s)}$ [Eq. (6)] was estimated as exothermic by 95 kJ mol^{-1}.

$$Ag^+[Al(pftb)_4^-]_{(s)} + 2S_{8(s)} \longrightarrow [Ag(S_8)_2]^+[Al(pftb)_4]^-_{(s)} \quad (6)$$

$[AgS_8][Al(hfip)_4]$ (2): A model for gaseous AgS_8^+: The geometry of the gaseous AgS_8^+ cation is still unknown. However, all quantum-chemical optimizations starting in C_1 symmetry from the $[AgS_8]^+$ geometry in **2** or one half of the $[Ag(S_8)_2]^+$ cation in **4** always led to a minimum of approximate C_{4v} symmetry (see above) with similar structural parameters as the AgS_8 unit in **2**. Therefore it appears reasonable to propose that gaseous $[AgS_8]^+$ has a C_{4v}-symmetric geometry like the one shown in Figure 5, calculated at the best computational level employed ((RI-)MP2/TZVPP).

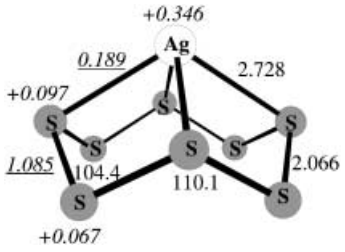

Figure 5. Fully optimized geometry of the C_{4v} $[AgS_8]^+$ cation at the (RI-)MP2/TZVPP level. Bond lengths are given in Å, computed partial charges are in italics, shared electron numbers (SEN) are shown in italics and underlined. For comparison S_8 (D_{4d}) at this level: S–S = 2.058 Å, S–S–S = 107.4°, SEN(S–S) = 1.089.

In agreement with this proposal, we showed by an analysis of the strengths of the Ag–X bond valences (X = S, O, F, see Table 1) that, in the molecular compound **2**, the more covalent interaction of the silver atom with the S_8 molecule is stronger (0.560 v.u.) than the ionic interaction with the $[Al(hfip)_4]^-$ anion (0.405 v.u.). Therefore, it is reasonable to use this almost C_{4v}-symmetric $\{AgS_8\}^+$ moiety in **2** or the calculated geometry as a model for the structure of the gaseous $[AgS_8]^+$ cation observed in the MS.[9] Since the Ag^+ ion in **2** is still coordinated by the $[Al(hfip)_4]^-$ anion, the average Ag–S bond length in **2** (2.924 Å) is longer than that between the naked Ag^+ ion and the four sulfur atoms in C_{4v} $[AgS_8]^+$ in the gas phase (2.728 Å in Figure 5). The calculated sulfur partial charges of 0.067 to 0.097 are in good agreement with the observation of 10 S–F contacts in **2** (Table 1).

But how is the silver ion bonded to the S_8 molecule? In C_{4v} $[AgS_8]^+$ ionic and covalent bonding contributions lead to the same structure: the purely ionic case would clearly give the C_{4v} structure, as in Figure 5, since the number of contacts from the silver ion to the sulfur atoms is maximized in this geometry. An orbital-based interpretation comes to the same conclusion. One important component of the silver–sulfur bonding in C_{4v} $[AgS_8]^+$ is certainly the interaction of the spherical $5s^0$ Ag acceptor orbital (LUMO) with the HOMO of the S_8 molecule (MO representation of the $3p^2$ lone-pair orbitals of the sulfur atoms). This may be seen from the comparable energies of the Ag^+ LUMO at -0.230 a.u. and the S_8 HOMO at -0.373 a.u. (HF/TZVPP).[35] Secondary bonding contributions may arise from the interaction of the occupied sulfur $3p^2$ lone-pair donor orbitals with two of the empty silver $5p^0$ acceptor orbitals as in Figure 6.

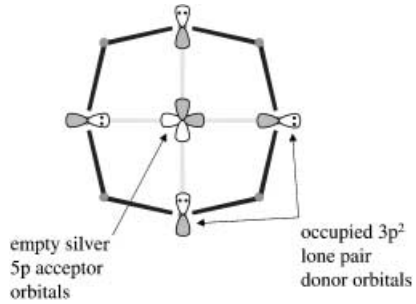

Figure 6. Top view of the C_{4v} $[AgS_8]^+$ cation: a suitable arrangement for the additional interaction of the occupied sulfur $3p^2$ lone-pair donor orbitals with two of the empty silver $5p^0$ acceptor orbitals. This leads to positive charge transfer from the silver atom to the sulfur atoms.

Such an interaction additionally reduces the positive charge residing on the silver atom. In agreement with this, the calculated positive partial charge assigned to the Ag atom of the $[AgS_8]^+$ cation in Figure 5 is very low, only 0.346, the rest is delocalized onto the coordinated S_8 ring. It may be noted that a similar experimental partial charge was assigned to the silver atom of the AgS_8 unit of **2**; based on the four Ag–O and Ag–F contacts of the $\{AgS_8\}$ moiety, the Ag atom has a positive charge of 0.405 v.u. (Table 1).[25]

The undistorted $[Ag(S_8)_2]^+$ cation: A model for the gas phase: The undistorted $[Ag(S_8)_2]^+$ cations in **3** (200 K) and **4** are presumably the best experimentally established models for the gaseous cation observed in MS experiment.[9] At 150 K the geometry in **3** is slightly distorted. On cooling from 200 to 150 K, the ordering process of the CF_3 groups of the anion led to a reorientation of the cation–anion contacts. Due to the decreased thermal energy available at 150 K, these S–F contacts now displace the cation slightly from the ideal minimum geometry.[36]

What is the global minimum of gaseous $Ag(S_8)_2^+$? The computational models employed here are not conclusive

  0947-6539/02/0815-3392 $ 20.00+.50/0 *Chem. Eur. J.* **2002**, *8*, No. 15

about the global minimum geometry of gaseous $[Ag(S_8)_2]^+$ and disagree already on the most favorable overall structure—BP86/TZVPP and B3LYP/TZVPP suggest the C_i isomer to be the most favorable minimum, but MP2 favors the more symmetric D_{4d} cation. However, the energetic differences are minimal (see Table 4). As shown earlier for other weakly bound systems,[37] the DFT and HF-DFT levels BP86 and B3LYP are intrinsically incapable of properly describing very weak dispersive interactions and, consistently, overestimate the strengths of the short, more covalent Ag–S bonds by ≥ 0.1 Å, but considerably underestimate the strengths of the very weak dispersive Ag–S interactions by 0.1–0.5 Å compared with the cations in **3** (200 K) or **4** (Table 3). The computationally relatively expensive MP2/TZVPP ab initio level, which accounts for 80 to 85% of the dispersive interactions,[38] such as those in the weak Ag–S contacts, performs better and gives structural parameters closer to the experiment (Table 3). However, since the overall geometry of the calculated $[Ag(S_8)_2]^+$ structures depends strongly on the correct description of the multitude of weak dispersive Ag–S interactions, the fine tuning to model the exact (less symmetric) position of the silver ion between the two S_8 rings was not achieved. Presumably a better description of the weak dispersive Ag–S interactions has to be provided by higher correlated methods such as MP3, MP4, or CCSD(T) and even more flexible basis sets. Due to computational and program limitations, it is currently impossible for us to employ better methods, and this work remains to be done.[39] Alternatively, one could argue that the geometries of the solid $[Ag(S_8)_2]^+$ cations in **3** (200 K) and **4** were distorted by packing effects, especially considering the flat potential-energy surface where large structural changes may only lead to small energetic changes (cf. 150 K and 200 K phases of **3**). However, the centrosymmetric geometry of the $[Ag(S_8)_2]^+$ cation was independently found with two conceptually very different anions: the "Teflon coated" $[Al(pftb)_4]^-$ anion with a surface built from CF_3 groups and the $[Sb(OTeF_5)_6]^-$ anion, which has a surface made from Te–F bonds. From the ellipsoid plot of the 200 K phase of **3** (deposited), it is evident that all the CF_3 groups are freely rotating around the C–C bond, and at least one entire $C(CF_3)_3$ group is also rotating around the C–O vector. This suggests that the cation–anion interactions and thus packing effects in **3** (200 K) are minimal, and that the centrosymmetric geometry of the $[Ag(S_8)_2]^+$ cation, as in **3** (200 K) and **4**, also represent the global minimum of the gaseous $[Ag(S_8)_2]^+$ cation. We suggest that higher correlated calculations will confirm this conclusion.[39]

Analysis of the structural data: Due to the lack of a computed geometry very close to the experimental structure, we concentrate in the following on the analysis of the experimental data and only refer to the computation when appropriate. The primary coordination of the silver atom of the undistorted $[Ag(S_8)_2]^+$ cation may be described as linear dicoordinate or alternatively as planar (see above). Both descriptions and the similar ionization potentials $IP(Ag) = 731$ and $IP(S_8) = 872$ kJ mol^{-1}[53] suggest that this bonding is not entirely due to electrostatic contributions, for which a more regular at least C_4 symmetric cation would be expected (cf. D_{4d} $[Ag(S_8)_2]^+$ in Figure 4a and Table 5). Therefore orbital-based interactions have to play an important role in the Ag–S bonding. Due to the coordination to the Ag^+ ion, all S_8 rings in **1**–**4** are positively polarized, that is, they exhibit contacts to the fluorine atoms of the anions that are shorter than the sum of their respective van der Waals radii. An analysis of the S–F solid-state contacts showed that not only the formally positively charged tricoordinated sulfur atoms form contacts but also most of the formally neutral dicoordinate sulfur atoms. Figure 7 summarizes the sulfur partial

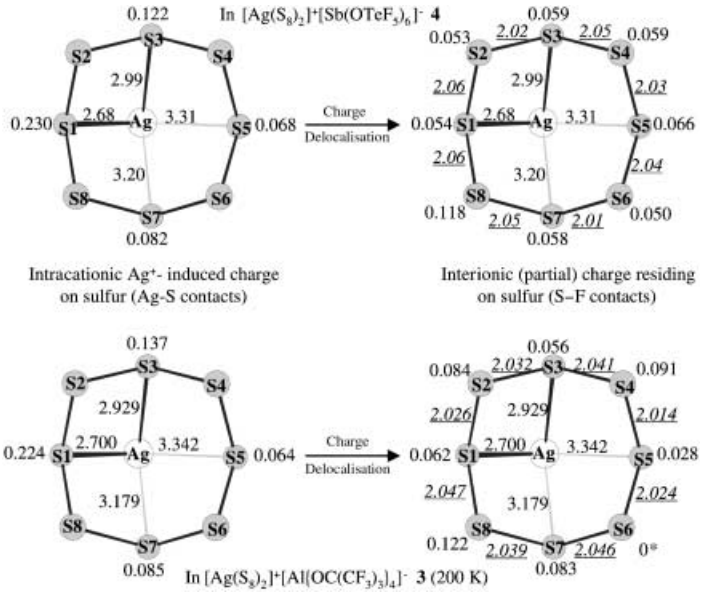

Figure 7. Observed intra- and interionically induced partial charges residing on the S_8 ring of the centro- or almost centrosymmetric $[Ag(S_8)_2]^+$ cation in a top view. For clarity the geometry of the almost centrosymmetric $[Ag(S_8)_2]^+$ cation in **3** (200 K) was averaged by assuming centrosymmetry and the symmetry equivalent halves were omitted. S–S bond lengths (underlined and in italics) are given in Å, (S–S standard deviation: 0.008 (**3**) or 0.02 (**4**) Å). * No S–F contacts.

charges of the undistorted centrosymmetric or almost centrosymmetric $[Ag(S_8)_2]^+$ cations in **3** and **4**, as induced by intracationic Ag–S and interionic S–F contacts based on Brown's bond valence method.[25] The lengths, and therefore also the strengths, of the intracationic (interionic) Ag–S (S–F) contacts in v.u. reflect the amount of positive charge transferred from the Ag^+ ion to the coordinated sulfur atoms (the coordinated sulfur atoms to the fluorine atoms of the anion).

This analysis gives the highest intracationic induced sulfur partial charges on S1 and S3, corresponding to the shortest Ag–S contacts (0.122 to 0.230 v.u., Figure 7). However, the interionic S–F separations imply that the sulfur partial charges are almost evenly spread over all the sulfur atoms and range from 0.028 to 0.122. Note that S1 and S3, with the shortest Ag–S contacts, bear relatively little positive charge based on the S–F contacts. Moreover, we find the highest interionic partial charges of 0.118 and 0.122 residing on the formally neutral dicoordinate atom S8 (Figure 7). The regular distribution of the interionic sulfur partial charges indicates some kind of orbital-based charge delocalization from the tricoordinate S_{Ag} to the dicoordinate S atoms. However, the

S–S bond lengths are only very slightly influenced during this process (Figures 8 and 12, below). To obtain meaningful average S–S lengths of the coordinated S_8 rings of all the structurally characterized $\{Ag(S_8)_2\}$ moieties, they were brought into an orientation as shown in Figure 8. Then we obtained the average S–S bond length for each type of S–S bond within the ring (see Supporting Information for details).

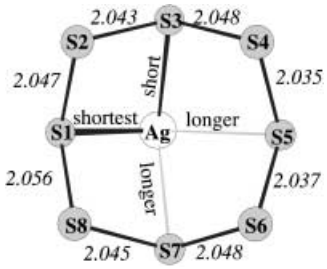

Figure 8. Average S–S bond lengths of seven S_8 rings coordinated to a Ag^+ ion in $[Ag(S_8)_2][AsF_6]$ and **1, 3**, and **4**. To allow for a comparison of the S–S lengths, all $\{AgS_8\}$ moieties had the same orientation of the Ag–S contacts, that is, the shortest contact was to S1, the second shortest to S3, and the two longer contacts to S5 and S7 (labeling as in this Figure).

The average separations between the different types of S–S bonds in Figure 8 differ only by a maximum of $\Delta(d(S–S)) = 0.021$ Å. However, some statistically meaningful features may be noted from Figure 8. The longest average S1–S8 bond incorporates S1 that has the shortest contact to the silver atom. The shortest S5–S6 and S5–S4 bonds are found around the weakly silver-coordinated S5 atom with the largest possible separation from S1. There is a slight long-short-long-short S–S bond length alternation starting from S1. This observed alternation is supported by the calculations collected in Table 3, which all show this small S–S bond length alternation with $\Delta(d(S–S)) = 0.031 – 0.039$ Å.

A bonding model: From first principles it is clear that the bonding in $[Ag(S_8)_2]^+$ has an ionic and a covalent contribution. A purely ionic bonding interaction would lead to a highly symmetric structure in which the coulombic interactions are maximized (i.e. at least C_4 symmetry) and a purely covalent bonding would lead to a geometry that is determined by the geometric restrictions imposed on the species by maximizing the orbital overlap between the Ag^+ and S_8 orbitals. As seen from the shallow potential energy surface of the cation, both ionic and covalent contributions are of importance for the description of the bonding of the $Ag(S_8)_2^+$ cation. Important orbitals involved in the bonding are the occupied $3p^2$ lone-pair donor orbitals of S_8 (= HOMO) and the empty $5s^0$ and $5p^0$ acceptor orbitals of the silver ion (= LUMO and LUMO+1). At this point we note that there is ongoing controversy about the importance of (n + 1)p-orbital contributions to the bonding of nd metals.[40a–d]

To a first order of approximation, the $[Ag(S_8)_2]^+$ cations in **3** (200 K) and **4** are linear dicoordinate. It was shown for linear $M(CO)_2^+$ complexes[41a] (M = Cu, Ag, Au) as well as other linear d^{10} coinage-metal systems[41b,c] that the preferential linear arrangement is induced by a sd hybridization (see ref. [42] for a bonding model). However, we concluded[42] that an alternative description that does not require the unusual polarization of the closed $4d^{10}$ shell of the silver ion is more likely.[42] Similarly to the situation in C_{4v} $[AgS_8]^+$, the interaction of the spherical $5s^0$ Ag acceptor orbital with the occupied $3p^2$ lone-pair donor orbitals of the S_8 molecule is a strong component of the silver–sulfur bonding in undistorted $[Ag(S_8)_2]^+$. However, it is improbable that only the empty spherical $5s^0$ Ag orbital acts as an acceptor, since this would lead to a very regular structure, that is, to an at least C_4 symmetrical $[Ag(S_8)_2]^+$ cation, which would also be expected to be the minimum structure of an exclusively ionically bonded $[Ag(S_8)_2]^+$ cation. Due to the lower symmetry of the observed structure, it is likely that the empty $5p^0$ orbitals are also involved in the covalent Ag–S bonding (cf. $[AgS_8]^+$ above). Figure 9 shows a MO representation of the possible bonding interaction between the empty Ag $5p^0$ acceptor orbitals and the occupied S $3p^2$ lone pair donor orbitals in the cation.

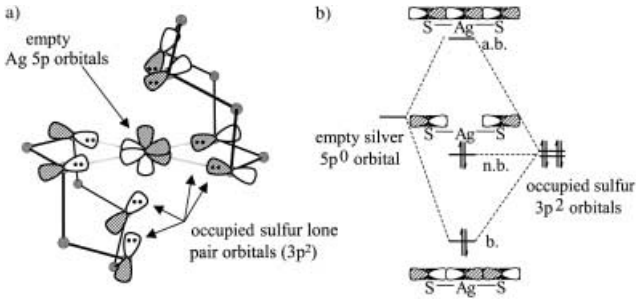

Figure 9. a) Ag 5p orbital participation in the covalent Ag–S bonding: donation of electron density from the occupied $3p^2$ sulfur lone-pair orbitals to the empty $5p^0$ silver orbitals, and transfer of positive charge from the silver to the coordinated sulfur atoms. b) The resulting set of one bonding (b.), one nonbonding (n.b.) and one antibonding (a.b.) molecular orbital for one linear S-Ag-S unit.

The empty Ag $5p^0$ acceptor orbital lying at the lowest energy interacts strongest with two of the S $3p^2$ lone-pair donor orbitals leading to a primary linear silver coordination with two comparatively strong Ag–S bonds at about 2.68–2.71 Å as shown in Figure 9b.[43] This 3-center/4-electron bonding resembles the situation in XeF_2 or I_3^-, in which the same three molecular orbitals are responsible for the bonding.[44] The next strongest set of Ag–S bonds, at about 2.92–2.99 Å, leads to the "planar" conformation and arises from the interaction of the next energetically favorable orthogonal Ag $5p^0$ acceptor orbital with two $3p^2$ lone-pair donor orbitals of sulfur atoms in a suitable orientation (1,3 coordination, Figure 10a). The energetic separation between the donor ($3p^2$) and the acceptor ($5p^0$) orbital in this secondary interaction is larger and, therefore, the Ag–S bond is longer. Due to symmetry,[45] steric hindrance, and a further increased energetic separation, the last remaining empty Ag 5p acceptor orbital interacts only weakly with the four occupied S $3p^2$ lone-pair donor orbitals left and consequently the last Ag–S contacts are long and range from 3.18 to 3.35 Å. The correct description of this last, very weak bonding interaction is crucial for obtaining the correct geometry in the quantum chemical optimization (see below). An interaction as shown in

  0947-6539/02/0815-3394 $ 20.00+.50/0 *Chem. Eur. J.* **2002**, *8*, No. 15

Figure 9 transfers the positive charge from the Ag^+ cation onto the coordinated sulfur atoms S_{Ag} (cf. intracationic sulfur partial charges in Figure 7). Consistently, all calculated partial charges of the Ag atom within the $[Ag(S_8)_2]^+$ cation are very low and range from +0.23 to +0.29 (all levels and TZVPP basis set).

A bonding interaction that describes the delocalization of the positive charge within the S_8 ring is still missing (cf. interionic sulfur partial charges in Figure 7). Due to the small range of the average S–S bond lengths of 2.035–2.056 Å (Figure 8) and the orthogonal orientation of the adjacent 3p orbitals in the coordinated S_8 ring, $3p_\pi - 3p_\pi$ bonding, as often found in the homopolyatomic sulfur or binary sulfur halogen cations,[30, 46] is probably *not* the reason for this charge delocalization.[47] Another interaction observed in polysulfur chemistry is the $3p^2 \rightarrow 3\sigma^*$ bonding which accounts for additional charge delocalization in S_7[48] as well as in S_8^{2+}.[30, 46a] With this interaction, electron density from an occupied S $3p^2$ lone-pair donor orbital is transferred to the empty $3\sigma^*$ acceptor orbital of a vicinal S–S bond. This interaction accounts for further charge delocalization, as shown in Figure 7. A MO-based representation of this $3p^2 \rightarrow 3\sigma^*$ delocalization process within the S_8 ring is shown in Figure 10.

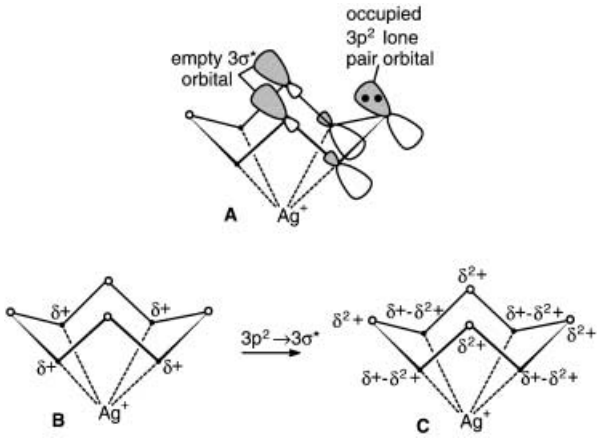

Figure 10. Positive-charge delocalization in the S_8 rings of $[Ag(S_8)_2]^+$ achieved by a $3p^2 \rightarrow 3\sigma^*$ interaction. Transfer of positive charge from the coordinated sulfur atoms to the uncoordinated sulfur atoms.

The starting point for the delocalization is **B**. Electron density is transferred—as in Figure 9—from the occupied S $3p^2$ lone-pair orbitals to the Ag^+ ion. Correspondingly, the sulfur atoms are left positively charged, as shown in **B**. Positive charge is further delocalized onto the dicoordinate sulfur atoms by donation of electron density from the occupied S $3p^2$ lone-pair orbitals into the empty $3\sigma^*$ orbital of the vicinal S–S bonds as illustrated in **A**. In total this leads to positive (partial) charges on all sulfur atoms as in **C** (cf. Figure 7 above and Figure 11 below). Most of the bond shortening and lengthening induced by the multiple $3p^2 \rightarrow 3\sigma^*$ interactions in $[Ag(S_8)_2]^+$ cancel out due to the only slightly distorted D_{4d} symmetry of the S_8 rings; however, the overall energy is lowered by this positive charge delocalization process. The small bond-length alternation within the S_8 ring, as evident from Figure 8 and the calculations (Table 3), is due to the differing strengths of the Ag–S contacts, which lead to differing partial charges induced on the coordinated S_{Ag} atoms. Therefore, depending on the amount of positive charge induced on the S_{Ag} atom, the multiple $3p^2 \rightarrow 3\sigma^*$ interactions vary in strength leading to different S–S bond lengths. This is also reflected in the calculated SENs of the S–S bonds and the calculated partial charges on the sulfur atoms in the best optimized geometry (MP2/TZVPP), shown in Figure 11.

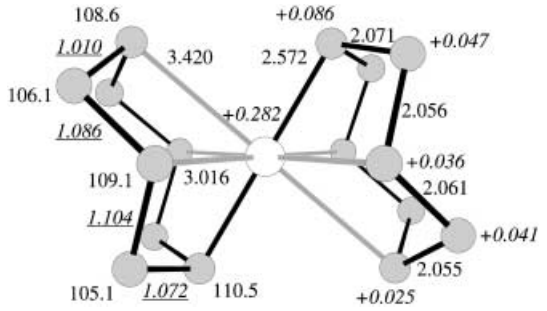

Figure 11. Fully optimized geometry of the C_{2h} $[Ag(S_8)_2]^+$ cation at the (RI-)MP2/TZVPP level. Bond lengths are given in Å, bond angles in degrees, computed partial charges are shown in italics, SENs are shown in italics and underlined. For comparison S_8 (D_{4d}) at this level: S–S = 2.058 Å, S-S-S = 107.4°, SEN(S–S) = 1.089.

"Pseudo-Gas-Phase Conditions" in the Solid State: Large and weakly coordinating anions stabilize salts that contain unusual and undistorted cations such as O_2^+,[49, 50] X_2^+ (X = Br, I),[30] Xe_2^+,[51] HC_{60}^+,[52] $[Ag(P_4)_2]^+$,[15] and $Ag(S_8)_2^+$ that were initially observed in the gas phase by mass spectrometry. How can this be understood? All the anions employed are stable toward oxidation, very nonbasic, and the single negative charge is dispersed over many atoms; this eliminates anion decomposition as well as strong and structure determining cation–anion contacts (cf. **1**). Since lattice energies are inversely proportional to the sum of the ionic radii (or volumes) of the constituting ions, the lattice energies of the obtained salts are very low (Scheme 1 and Table 8). In fact,

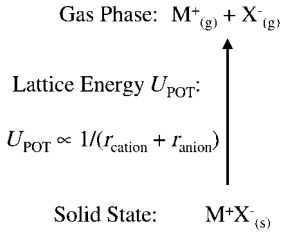

Scheme 1. The difference between solid state and gas phase: the lattice potential energy.

they are so low that the lattice energy of **3** of 326 kJ mol^{-1} approaches the values of sublimation enthalpies of molecular solids of comparable atomic weight, that is, of C_{60} or C_{70} of 175 or 200 kJ mol^{-1} (cf. M_r(**3**) = 1588 vs. 721 (C_{60}) and 841 (C_{70}) g mol^{-1}).[53, 54] Comparing the lattice energy of **3** with the lattice energies of typical salts such as LiF (1036 kJ mol^{-1})

Table 8. Thermochemical volume and lattice potential energies of several M^+X^- salts.

Salt	V_{therm} [Å^3]	U_{pot} [kJ mol^{-1}]
LiF	27	1036[a]
CsF	43	740[a]
$Cs[AsF_6]$	128	568[b]
$Cs[Al(pftb)_4]$	776	362[b]
$[Ag(S_8)_2][Al(pftb)_4]$	1169	326[b]

[a] Experimental value.[53] [b] Calculated from the thermochemical volumes.[28]

and CsF (740 kJ mol^{-1}) shows clearly that the environment of the ions in $Ag(S_8)_2^+[Al(pftb)_4^-]$ more closely resembles the situation in the gas phase (or a molecular solid) than the strong electrostatic field within a classical salt, as in LiF or CsF. Therefore, we call the environment of the cations within the framework of an ensemble of very weakly coordinating anions such as $[Al(pftb)_4]^-$ or $[Sb(OTeF_5)_6]^-$ "pseudo-gas-phase conditions" in the solid state.

Apart from being weakly basic and stable to oxidation, another stabilizing term for weak Lewis acid base adducts $[AgL_2]^+[X^-]$ ($X^- =$ suitable anion) arises from using large counterions—reduced gain in $Ag^+[X^-]$ lattice energy upon dissociation of $[AgL_2]^+[X^-]$ into $Ag^+[X^-]$ and 2 L (see Scheme 2 for the Born–Haber cycle).

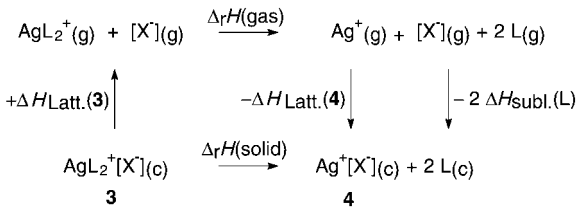

Scheme 2. Born–Haber cycle for the dissociation of a solid Lewis acid base adduct $[AgL_2]^+[X^-]$ into $Ag^+[X^-]$ and 2 L.

Let us consider two cases: $L = S_8$ and $X^- = [AsF_6]^-$ or $[Al(pftb)_4]^-$. The calculated lattice potential enthalpies for $[Ag(S_8)_2]^+[X^-]$ are 393 and 327 kJ mol^{-1}, those of $Ag^+[X^-]$ are 586 and 361 kJ mol^{-1} (thermochemical volumes).[28] The gas-phase enthalpy $\Delta_r H$(gas) and the sublimation enthalpy of S_8 are the same in both cases, and therefore the only differences are due to the lattice energies. For $X = AsF_6^-$, the resulting gain in lattice energy upon dissociation is 193 kJ mol^{-1}, while that for $X = [Al(pftb)_4]^-$ is only 34 kJ mol^{-1}. Therefore $[Ag(S_8)_2]^+[Al(pftb)_4^-]$ is more stable by 159 kJ mol^{-1} against a dissociation as in Scheme 2 than the $[AsF_6]^-$ salt. In other words, with the $[Al(pftb)_4]^-$ anion one can stabilize $[AgL_2]^+$ Lewis acid base adducts of very weak bases L for which the gas-phase term $[Ag(L)_2]^+_{(g)} \rightarrow Ag^+_{(g)} + 2\,L_{(g)}$ is less endothermic than that with the $[AsF_6]^-$ anion by about 100–160 kJ mol^{-1}.

Many other simple cations of fundamental interest may be stabilized by using "pseudo-gas-phase conditions" in the solid state, that is, weak Lewis acid base adducts as well as highly electrophilic cations such as $[P_5X_2]^+$ ($X = Br$, I)[55] or $[AgSe_6]^+$[56] and S_5^+[57] hitherto unknown in the solid state.

Conclusion

The concept of "pseudo-gas-phase conditions" in the solid state allowed us to stabilize the first examples of undistorted homoleptic metal–S_8 complexes, that is, the almost C_{4v}-symmetric $Ag(\eta^4\text{-}S_8)^+$ and the approximately centrosymmetric $[Ag(\eta^4\text{-}S_8)_2]^+$ cation. Their geometries are the best approximation of the structure of the gaseous $[AgS_8]^+$ and $[AgS_{16}]^+$ cations observed by MS methods.[9] A new generation of very weakly coordinating anions (WCAs) of type $[Al(OR_f)_4]^-$ ($OR_f =$ polyfluorinated aliphatic alkoxide)[11] was used to stabilize the cations, and the results obtained showed that the $[Al(pftb)_4]^-$ anion[11] is an at least as good WCA as $[Sb(OTeF_5)_6]^-$, while being much easier to prepare[11] and handle[58] on a large scale. Similarly to the situation in the $[Ag(\eta^2\text{-}P_4)_2]^+$ cation,[15] unusual weak bonding interactions in $[Ag(\eta^4\text{-}S_8)]^+$ and $[Ag(\eta^4\text{-}S_8)_2]^+$ could be stabilized by WCAs. However, the $[Ag(\eta^2\text{-}P_4)_2]^+$ and $[Ag(\eta^4\text{-}S_8)_2]^+$ bonding differs considerably. Due to the availability of sulfur $3p^2$ lone-pair orbitals in S_8, only an additional $3p^2 \rightarrow 5p^0$ *donation* resulted, which leaves very little positive charge on the Ag atom (+0.23 to +0.29). *tetrahedro*-P_4 has *no* $3p^2$ lone pairs and is even more reluctant to bear positive charge than sulfur (cf. homopolyatomic sulfur cations are known,[30] those of P are still unknown in condensed phases). Consistently the $4d^{10} \rightarrow 3\sigma^*$ *back donation*[13] reduces the charge residing on the phosphorus atoms and leaves more positive charge on the silver atom (+0.74 according to ref. [15b]). The multitude of weak dispersive Ag–S interactions in $[Ag(\eta^4\text{-}S_8)_2]^+$ is difficult to model computationally, and the DFT or HF-DFT levels BP86 and B3LYP, which are intrinsically incapable of describing weak interactions, failed to give satisfying geometries of the $[Ag(\eta^4\text{-}S_8)_2]^+$ cation. Only the rather expensive MP2/TZVPP level is able to account for most of the weak bonding and gave geometries closest to the experimental data. However, it still remains to be seen if the global minimum of the gaseous $[Ag(\eta^4\text{-}S_8)_2]^+$ cation is D_{4d}-, C_{2h}- or C_i-symmetric as in the experiment. We are confident that higher correlated methods such as MP3, MP4, or CCSD(T) with flexible basis sets will reproduce the experimental C_i minimum; however, due to program limitations and lack of computational power for us this is impossible to achieve currently.[39] In this respect C_i $[Ag(\eta^4\text{-}S_8)_2]^+$ may in future serve as a test case for modeling weak interactions.

Experimental Section

All manipulations were performed by using standard grease-free Schlenk or dry-box techniques and a dinitrogen or argon atmosphere. Reactions were carried out in a two-bulb glass vessel incorporating a medium or fine sintered-glass frit, one or two J. Young valves and a Teflon-coated stirring bar as described in ref. [59]. All reactions with $AgSbF_6$ were handled in the dark in glass vessels wrapped in aluminum foil. FT-Raman spectra were obtained at RT from neat samples sealed under a dinitrogen atmosphere in dried melting point capillaries or 5 mm NMR tubes on an FTIR spectrometer (Bruker IFS-66) equipped with a FT-Raman accessory (Bruker FRA-106) and with a Nd–YAG laser (1064 nm irradiation, 4 cm^{-1} resolution). NMR spectra of sealed samples were run in CD_2Cl_2 on a Bruker AC250 spectrometer and were referenced to the solvent (^{1}H, ^{13}C) or external aqueous $^{27}AlCl_3$. The silver aluminates $AgAl(OR)_4$ were

  0947-6539/02/0815-3396 $ 20.00+.50/0 *Chem. Eur. J.* **2002**, *8*, No. 15

prepared according to the literature.[15] Sulfur (BDH, precipitated, 99%) was vacuum dried before use. $AgSbF_6$ (Aldrich, 98%) was used as received. SO_2 and SO_2ClF (Matheson) were distilled onto and stored over CaH_2 or molecular sieves (4 Å), respectively, at least 24 hours prior to use. CH_2Cl_2 (Anachemia Science, 99.5% min.) and CS_2 (UV grade) were stirred over P_4O_{10} for two days with four additions of fresh P_4O_{10} and then distilled onto and stored over molecular sieves (4 Å) or CaH_2.

Synthesis of $[Ag(S_8)_2][SbF_6]$ (1): Elemental sulfur (0.97 g, 3.78 mmol, 1.6% excess) and $AgSbF_6$ (0.64 g, 1.86 mmol, limiting reagent) were placed into one bulb of a two-bulb vessel. SO_2 (15 g) was condensed onto the solids, and the mixture was stirred for 1 day at room temperature; this resulted in a pale orange solution over a large amount of a white to pale orange solid. The solution was filtered into the other bulb and then repeatedly condensed (21×, 7 days) back onto the solid mass to leave no soluble material only an insoluble microcrystalline product. The solvent was slowly removed, and close examination of the recovered solid (total 1.66 g, expected 1.59 g) under the microscope revealed the presence of a few yellow crystals that did not decompose when brought in contact with the atmosphere and were probably the remaining excess sulfur (expected 0.02 g). The crystals were physically removed, and the remaining white to pale orange microcrystalline product **1** was characterized by FT-Raman spectroscopy (see Table S5 and Figure S5 in the Supporting Information). Raman: $\tilde{\nu}(Ag(S_8)_2^+)$ (%) = 476 (70), 468 (50), 441 (13), 421 (1), 262 (10), 255 (2), 246 (2), 224 (70), 220 (30), 203 (1), 167 (20), 157 (100), 92 (15) cm^{-1}; $\tilde{\nu}(SbF_6^-)$ (%) = 642 (10, $\tilde{\nu}_1$), 278 (10, $\tilde{\nu}_5$) (cm^{-1}). Compound **1**, which was insoluble in SO_2 turned dark brown in daylight (1 day); this probably indicated decomposition (possibly to Ag_2S or Ag). Samples were stored in the dark without noticeable decomposition in sealed glass tubes under nitrogen at −20 °C over a period of at least 2 years. Single crystals of **1** resulted from the light-induced disproportionation of $[C_{11}H_7S_3]^+[SbF_6^-]$ that formed from the reaction of $Ag[SbF_6]$ and $C_{11}H_7S_3Cl$; possibly as shown in equations S1 to S3 in the Supporting Information.

Synthesis of $[AgS_8][Al(hfip)_4]$ (2): In a typical preparation $AgAl(hfip)_4$ (0.530 g, 0.660 mmol) and S_8 (0.169 g, 0.660 mmol) were weighed into one bulb of a two-bulb vessel. Pentane (10 mL) was added to the mixture, and the resulting suspension was exposed to ultrasound for 1 h, with warming to approximately 30–40 °C. A colorless solution over very little grayish precipitate resulted and was filtered. Successive reduction of the volume of the filtrate to about 3 mL and cooling to −30 °C led to the formation of a large amount of colorless, very air- and moisture-sensitive single crystals of **2**, which grew to dimensions of up to 10×10×5 mm (0.586 g, 84%). ^{1}H NMR (250 MHz, CD_2Cl_2, 25 °C): $\delta = 4.49$ (sept., $^3J_{HF} = 5.7$ Hz); ^{13}C NMR (63 MHz, CD_2Cl_2, 25 °C): $\delta = 70.6$ (sept., $^2J_{CF} = 32.8$ Hz), 122.3 (q, CF_3, $^1J_{CF} = 283.5$ Hz); ^{27}Al NMR (78 MHz, CD_2Cl_2, 25 °C): $\delta = 59.1$ (s, $\tilde{\nu}_{1/2} = 200$ Hz); elemental analysis calcd (%) for $AgAlC_{12}F_{24}H_4O_4S_8$: Ag 10.18, Al 2.55; found Ag 10.0, Al 1.9.

Synthesis of $[Ag(S_8)_2]^+[Al(pftb)_4]^-$ (3): In a typical reaction, $[AgCH_2Cl_2][Al(pftb)_4]$ (0.294 g, 0.25 mmol), S_8 (0.130 g, 0.50 mmol), and CH_2Cl_2 (4 mL) were placed into one bulb of a two-bulb vessel. The suspension was exposed to ultrasound for 1 h with warming to approximately 30 to 40 °C, after which a clear colorless solution over very little grayish precipitate was obtained. The mixture was filtered, and the solvent removed in a dynamic vacuum until the filtrate had an very dense oily consistency (only very small amounts of CH_2Cl_2 left). This oil was stored overnight at +7 °C, after which a large amount of colorless crystals of **3** had formed within a few drops of CH_2Cl_2. The solvent was quickly decanted, and the crystals dried in a dynamic vacuum and isolated. Yield: 0.387 g (91%); ^{13}C NMR (63 MHz, $CDCl_3$, 25 °C): $\delta = 121.45$ (q, $J = 293.3$ Hz, CF_3); ^{27}Al NMR (300 MHz, $CDCl_3$, 25 °C): $\delta = 34.1$ ($\tilde{\nu}_{1/2} = 6$ Hz); elemental analysis calcd (%) for $AgAlC_{16}F_{36}O_4S_{16}$: Ag 6.79; found Ag 6.9.

Reaction leading to single crystals of $[Ag(S_8)_2][Sb(OTeF_5)_6]$ (4): SO_2 (3.57 g) was condensed onto $Ag[Sb(OTeF_5)_6]$[60] (0.666 g, 0.401 mmol) and a mixture of sulfur bromides [S_8 (0.0314 g, 0.1224 mmol) preheated with Br_2 (0.0462 g, 0.2891 mmol) to give a yellowish brownish oil] in a 10 mm (o.d.) thick-walled NMR tube. On warming the mixture to RT an intensely red-orange solution over some fine colorless precipitate was obtained. The solution was decanted by a direct connection[61] into a one-bulb vessel (4.26 g solution) leaving an insoluble, beige material (0.1208 g) in the NMR tube. SO_2ClF (4.99 g) was condensed onto the soluble materials giving a reddish solution. Various attempts to grow crystals by successively reducing the volume of the solvent were unsuccessful. All volatile materials were removed in vaccuo to give a brown solid that gave a very poor FT-Raman spectrum (fluorescence). SO_2ClF (0.75 g) was condensed onto the residue (0.4699 g). Cooling the solution for 4 days to +5 °C afforded colorless crystals, which were shown by X-ray crystallography to be **4**. One of the colorless crystals was placed in a capillary, and a FT-Raman spectrum of this material showed strong fluorescence but the absence of S_8.

X-ray crystal-structure determinations: Data collection for X-ray structure determinations was performed on a Bruker AXS P4/SMART1000 (**1**), STOE IPDS (**3** 150 K, **3** 200 K, S_8), STOE STADI4 (**2**) or RIGAKU AFC5R (**4**) diffractometer with graphite-monochromated $Mo_{K\alpha}$ (0.71073 Å) radiation. Single crystals of **1**–**3** and S_8 in perfluoroether oil were mounted on top of a glass fiber and then brought into the cold stream of a low-temperature device so that the oil solidified. A hemisphere of data of **1** was collected by using ω and θ scans with a scan width of 0.3° and 10 s exposure times. The detector distance was 6 cm. The raw data frames indicated multiple twinning, and routine indexing failed. The orientation matrix of the major component was obtained manually (RLATT), the data were indexed and reduced (SAINT)[62] and corrected for absorption (SADABS).[63] Calculations for **1**–**3** and S_8 were performed on PCs by using the *SHELX97* software package.[64] Initially for **3** (200 K) the centrosymmetric space group $P2_1/m$ was chosen, giving a centrosymmetric $[Ag(S_8)_2]^+$ cation, but the agreement factors only converged at $R1 = 0.1009$. From the 150 K determination of **3**, it was evident that the chiral space group $P2_1$ was correct at this temperature, and the lattice exceptions of the 200 K determination also fitted better to $P2_1$. Therefore this space group was also checked for the 200 K structure of **3** and led to better agreement factors of the 200 K structure of $R1 = 0.0895$. This suggests that at higher temperatures than 200 K a phase transition to a centrosymmetric monoclinic phase ($P2_1/m$) may occur. The anions in **3** exhibit rotational disorder of the CF_3 groups as well as one entire $C(CF_3)_3$ group. Therefore three fluorine and three carbon atoms were split over two positions; this resulted in site occupation factors of 40–45% (figure deposited). A series of 151 SADI and FREE restraints had to be used in **3** to assign reasonable structural parameters to the CF_3 groups. However, the cations in **3** are well behaved. A crystal of **4** was mounted in a glass capillary and sealed under an atmosphere of dry nitrogen as previously described.[65] The cell constants and an orientation matrix for data collection of **4** were obtained by least-square refinement of 24 carefully centered reflections in the range of $38.16° < 2\Theta < 39.86°$. Data were collected in the $\omega - 2\Theta$ scan technique up to a maximum of 2Θ of 60.1° with an ω scan width of $1.63+0.35\tan\Theta°$ at a scan speed of 16° min^{-1}. Weak reflections ($I < 15\sigma$) were rescanned up to a maximum of six scans, and the counts were accumulated. Stationary background counts were recorded on each side of the reflection with a peak/background counting time ratio of 2:1. The intensities of three representative standard reflections were measured every 150 reflections and decreased during the data collection by 4.5%. A linear correction factor was applied to account for this phenomenon. An empirical absorption correction, using the program DIFABS,[66] was applied. The refinement of **4** was done with the TEXSAN[67] crystallographic software package. All data were corrected for Lorentz and polarization effects. All structures were solved by direct methods and successive interpretation of the difference Fourier maps, followed by least-squares refinement on F^2 (SHELXL97, **1**–**3**) or F (TEXSAN, **4**). All non-hydrogen atoms were refined anisotropically. Hydrogen atoms in the calculated positions were included into the refinement by a riding model. The solid state packing of **3** and **4** was drawn with *Diamond 2.1*. Relevant data concerning crystallography, data collection, and refinement details are compiled in Table 9. CCDC-177421 (**2**), 177422 (**3** 200 K), 177423 (**3** 150 K) contain the supplementary crystallographic data for this paper. These data can be obtained free of charge via www.ccdc.cam.ac.uk/conts/retrieving.html (or from the Cambridge Crystallographic Data Centre, 12 Union Road, Cambridge CB2 1EZ, UK; fax: (+44) 1223-336-033; or deposit@ccdc.cam.uk). Further details of the crystal-structure investigations of the purely inorganic compounds may be obtained from the Fachinformationszentrum Karlsruhe, 76344, Eggenstein-Leopoldshafen, Germany (fax: (+49) 7247-808-666; e-mail: crysdata@fiz-karlsruhe.de) on quoting the depository numbers CSD-412324 (**1**) and -412325 (**4**).

Computational details: All computations were done with the program TURBOMOLE.[68] The geometries of all species were optimized at the (RI-)BP86, B3LYP, and (RI-)MP2 levels[69, 70] with the triple-ζ valence polarization (two d and one f function) TZVPP basis set[71b] or partly with the

Table 9. Crystallographic and refinement details.

Compound	**1**	**2**	**3** (150 K)	**3** (200 K)	**4**
crystal size [mm]	0.28 × 0.15 × 0.05	0.6 × 0.6 × 0.6	0.6 × 0.4 × 0.3	0.4 × 0.3 × 0.3	0.14 × 0.10 × 0.08
formula	$AgF_6S_{16}Sb$	$C_{12}H_4AgAlF_{24}O_4S_8$	$C_{36}AgAlF_{36}O_4S_{16}$	$C_{36}AgAlF_{36}O_4S_{16}$	$AgF_{30}O_6S_{16}SbTe_6$
M_w	856.58	1059.48	1587.97	1587.97	2174.13
crystal system	Monoclinic	Triclinic	Monoclinic	Monoclinic	Triclinic
space group	*C*2/c	$P\bar{1}$	$P2_1$	$P2_1$	$P\bar{1}$
a [Å]	17.535(4)	10.887(2)	10.707(2)	10.722(2)	10.756(3)
b [Å]	7.8465(16)	10.979(2)	20.049(4)	19.997(4)	10.905(4)
c [Å]	15.675(3)	14.961(4)	10.957(2)	11.058(2)	10.456(2)
α [°]	90	100.00(2)	90	90	95.96(2)
β [°]	102.652(5)	96.31(3)	96.24(3)	95.94(3)	108.94(2)
γ [°]	90	109.73(2)	90	90	81.29(3)
V [Å^3]	2104.4(8)	1630.2(6)	2338.1(8)	2358.0(8)	1144.6(6)
Z	4	2	2	2	1
ρ(calc) [Mg m^{-3}]	2.704	2.158	2.256	2.237	3.154
μ [mm^{-1}]	3.840	1.319	1.340	1.329	5.641
abs. corr.	–	empirical	numerical	numerical	empirical
max/min Trans.	–	0.3525/0.5202	0.683/0.471	0.672/0.461	0.7114/1.0000
2θ [°]	50	54	52	50	60
T [K]	173	200	150	200	213
refl. collected	4628	17201	17459	9857	5372
refl. unique	1746	7072	4572	6644	5038
refl. observed (4σ)	1556	6274	3760	3880	1473
R (int.)	0.0580	0.0440	0.0438	0.0739	0.043
GOOF	1.050	1.079	0.972	0.964	1.94
final *R* (4σ)	0.0372	0.0439	0.0557	0.0895	0.058
final *wR2* (all data)	0.1002	0.1306	0.1450	0.2650	0.069[a]
larg. res. Peak [e Å^{-3}]	0.970	0.928	1.220	0.728	1.17

[a] $R_w = [\Sigma w(|F_o| - |F_c|)^2/\Sigma(w|F_o|^2)]^{1/2}$.

smaller split valence polarization SVP basis set.[71a] The 28 core electrons of Ag were replaced by a quasi-relativistic effective core potential.[72] Frequency calculations were only performed at the more affordable BP86/SVP level and, unless otherwise stated, all structures represent true minima without imaginary frequencies on the respective hypersurface. For selected species a modified Roby–Davidson population analysis was performed by using the MP2/TZVPP electron density. Approximate solvation energies (CH_2Cl_2 solution with $\varepsilon_r = 8.92$) were calculated with the COSMO model[73] at the BP86/SVP (DFT-)level by using the MP2/TZVPP geometries. Thermochemical evaluations include the zero point energy calculated at the BP86/SVP level and thermal corrections to the enthalpy and entropy at 298 K.[74, 75] $\Delta H_{(g)}$ ($\Delta G_{(g)}$) denotes the enthalpy (free energy) change in the gas phase at 298 K, values indexed with CH_2Cl_2 include the COSMO solvation energies, and approximate the solution behavior in CH_2Cl_2. Complete tables containing all necessary computed energies have been deposited.

Acknowledgement

We thank Prof. H. Schnöckel and Prof. R. Ahlrichs for valuable discussions and advice, Dipl. Chem. G. Stößer and Dipl. Chem. J. Bahlo for the many attempts to record the Raman spectra of **2** and **3**. Financial support from the German Science Foundation (DFG) and the Fonds der Chemischen Industrie (to I.K.) as well as from the NSERC (to J.P.) and the Petroleum Research Fund (to J.P.) are gratefully acknowledged. I.K. and J.P. thank the Alexander von Humboldt Stiftung for providing a Feodor-Lynen grant for I.K. in 1997–1999 and a travel research fellowship for J.P. in 2001.

[1] Crystal structure determination of $[Ag(S_8)_2]^+[Sb(OTeF_5)_6]^-$ (**4**).
[2] Crystal structure determination of $[Ag(S_8)_2][SbF_6]$ (**1**).
[3] Preparation and characterization of $[Ag(S_8)_2][SbF_6]$ (**1**).
[4] This work started during the postdoctoral stay of I.K. with J.P. at UNB in Canada, and compound **4** was prepared there as a disproportionation product by I.K. under J.P.'s supervision. The work with the aluminates and all quantum chemical calculations were done at the Universität Karlsruhe as part of I.K.'s habilitation thesis.
[5] J. L. Abboud, M. Herreros, R. Notario, M. Esseffar, O. Mo, M. Yáñez, *J. Am. Chem. Soc.* **1996**, *118*, 1126.
[6] J. L. Abboud, I. Alkorta, J. L. Davalos, J.-F. Gal, M. Herreros, P.-C. Maria, O. Mo, M. T. Molina, R. Notario, M. Yáñez, *J. Am. Chem. Soc.* **2000**, *122*, 4451.
[7] M. Lin, C. Liu, L. Zheng, *Wuli Huaxue Xuebao* **1995**, *11*, 266.
[8] See the HS_n^+ PES in J.-L. M. Abboud, M. Essefar, M. Herreros, O. Mo, M. T. Molina, R. Notario, M. Yáñez, *J. Phys. Chem. A*, **1998**, *102*, 1996, or the $Ag(P_4)_2^+$ PES in [15b] as well as the calculations in this contribution.
[9] a) I. G. Dance, K. J. Fisher, G. D. Willett, *Inorg. Chem.* **1996**, *35*, 4177; b) P. Liu, C. Han, Z, Gao, F. Kong, Q. Zhu, *J. Phys. Chem. B* **1999**, *103*, 3337.
[10] a) H. W. Roesky, M. Thomas, J. Schimkowiak, P. G. Jones, W. Pinkert, G. M. Sheldrick, *J. Chem. Soc. Chem. Commun.* **1982**, 895; b) H. W. Roesky, M. Witt, *Inorg. Synth.* **1986**, *24*, 72.
[11] I. Krossing, *Chem. Eur. J.* **2001**, *7*, 490.
[12] H. P. A. Mercier, J. C. P. Saunders, G. T. Schrobilgen, *J. Am. Chem. Soc.* **1994**, *116*, 2921, and references therein.
[13] D. M. Van Seggen, P. K. Hurlburt, O. P. Anderson, S. H. Strauss, *Inorg. Chem.* **1995**, *34*, 3453.
[14] T. S. Cameron, I. Krossing, J. Passmore, *Inorg. Chem.* **2001**, *40*, 2001.
[15] a) I. Krossing, *J. Am. Chem. Soc.* **2001**, *123*, 4603; b) I. Krossing, L. van Wüllen, *Chem. Eur. J.* **2002**, *8*, 700. Using molecular P_4S_3 as a ligand led to polymeric homoleptic $[Ag(P_4S_3)_2]_\infty^+$ cations, see: A. Adolf, M. Gonsior, I. Krossing, *J. Am. Chem. Soc.* **2002**, in press.
[16] However, S_8 cocrystallizes with other molecules and forms solid inclusion compounds, see references in [17] for an up-to-date overview.
[17] F. A. Cotton, E. V. Dikarev, M. A. Petrukhina, *Angew. Chem.* **2001**, *113*, 1569, *Angew. Chem. Int. Ed.* **2001**, *40*, 1521.
[18] a) Review: A. Pfitzner, *Chem. Eur. J.* **2000**, *6*, 1891; b) A. Pfitzner, E. Freudenthaler, *Angew. Chem.* **1995**, *107*, 1784; *Angew. Chem. Int. Ed. Engl.* **1995**, *34*, 1647; c) A. Pfitzner, E. Freudenthaler, *Z. Kristallogr.* **1995**, *210*, 59; d) A. Pfitzner, E. Freudenthaler, *Z. Kristallogr.* **1997**, *212*, 103; e) A. Pfitzner, S. Reiser, T. Nilges, *Angew. Chem.* **2000**, *112*,

  0947-6539/02/0815-3398 $ 20.00+.50/0

4328; *Angew. Chem. Int. Ed.* **2000**, *39*, 4160; f) A. Pfitzner, S. Reiser, *Inorg. Chem.* **1999**, *38*, 2451; g) A. Pfitzner, T. Nilges, H.-J. Deiseroth, *Z. Anorg. Allg. Chem.* **1999**, *625*, 201; h) A. Pfitzner, S. Zimmerer, *Z. Anorg. Allg. Chem.* **1995**, *621*, 969.

[19] Basic work that opened the field: a) J. Fenner, A. Rabenau, *Z. Anorg. Allg. Chem.* **1976**, *426*, 7; b) U. von Alpen, J. Fenner, B. Predel, A. Rabenau, G. Schluckebier, *Z. Anorg. Allg. Chem.* **1978**, *438*, 5; c) M. H. Möller, W. Jeitschko, *J. Solid. State Chem.* **1986**, *65*, 187; d) U. Thewalt, B. Müller, *Z. Naturforsch. B: Anorg. Chem. Org. Chem.* **1982**, *37*, 828.

[20] In the original publication [10a] these structure-determining Ag–F contacts were not recognized and, therefore, we show these contacts in Figure 1.

[21] Regardless of whether larger single crystals or ground powders were used in sealed m.p. or NMR tubes, the samples decomposed immediately in the LASER beam, turning black. After about 500–1000 scans, very weak bands of elemental S_8 were visible, which did not show up in the initial spectra (64 scans). Bands due to the anions were not observed.

[22] Containing traces of CH_2Cl_2.

[23] In the course of this investigation we (fortuitously) redetermined the solid-state structure of orthorhombic sulfur S_8 at 150 K. This solid-state structure is very good: $R1 = 0.0119$! (unpublished results) All comparisons were made to the structural data of this redetermination. S–S bond lengths [Å]: S1–S1A = 2.0503(7), S1–S2 = 2.0512(6), S2–S4 = 2.0510(6), S3–S4 = 2.0537(6), S4–S4A = 2.0464(8); bond angles [°]: S1A-S1-S2 = 108.98(2); S4-S2-S1 = 107.98(2), S2-S3-S4 = 107.30(2), S4A-S4-S3 = 108.34(2); torsion angles [°]: S1-S2-S3-S4 = 101.15(2), S2-S3-S4-S4A = 98.94(2), S3-S4-S4A-S3A = 96.82(2), S3A-S2A-S1A-S1 = 98.13(2).

[24] Holleman-Wiberg, *Lehrbuch der Anorganischen Chemie*, 101st ed. **1995**, Walter de Gruyter, Berlin.

[25] The contacts s (in valence units v.u.) have been defined as $s = (R/R_0)^{-N}$, in which R is the observed distance, R_0 is the covalent bond distance (bond order = 1) of the bond in question, and N is a empirically derived constant. For Ag(I)–F contacts $N = 6.5$ and $R_0 = 1.95$ Å, for Ag(I)–O $N = 7.4$, $R_0 = 1.946$ Å, for Ag(I)–S $N = 5.8$, $R_0 = 2.08$ Å, for S–F $N = 3.8$, $R_0 = 1.55$ Å. See: I. D. Brown in *Structure and Bonding in Crystals*, *Vol. 2* (Eds.: M. O'Keefe, A. Navrotsky), Academic Press, London, **1981**, p. 1.

[26] I. Krossing, H. Brands, R. Feuerhake, S. Koenig, *J. Fluor. Chem.* **2001**, *112*, 83.

[27] With the shortest Ag–M lengths in **3** and **4** of 8.048 Å (M = Sb), 8.148 Å (M = Al, 150 K) or 8.179 Å (M = Al, 200 K), the thermochemical radius of the $Ag(S_8)_2^+$ cation is 3.258 (**4**), 3.423 (**3**, 150 K) or 3.454 Å (**3**, 200 K)—on average 3.378 Å. With the unit cell parameters of **3** and **4** (see Table 9), the thermochemical volume of the $Ag(S_8)_2^+$ is 420 (**4**), 411 (**3**, 150 K) or 421 Å^3 (**3**, 200 K)—on average 417 Å^3.

[28] H. K. Roobottom, H. D. B. Jenkins, J. Passmore, L. Glasser, *Inorg. Chem.* **1999**, *38*, 3609.

[29] T. S. Cameron, I. Dionne, H. D. B. Jenkins, S. Parsons, J. Passmore, H. K. Roobottom, *Inorg. Chem.* **2000**, *39*, 2042.

[30] S. Brownridge, H. D. B. Jenkins, I. Krossing, J. Passmore, H. K. Roobottom, *Coord. Chem. Rev.* **2000**, *197*, 397, and references therein.

[31] a) H. D. B. Jenkins, L. C. Jitariu, I. Krossing, J. Passmore, R. Suontamo, *J. Comp. Chem.* **2000**, *21*, 218; b) I. Krossing, J. Passmore, *Inorg. Chem.* **1999**, *38*, 5203.

[32] When a solution of $[Ag(P_4)_2]^+[Al(pftb_4^-]$ in CH_2Cl_2 was added to S_8, and the mixture was exposed to ultrasonic enhancement, the S_8 remained unreacted at the bottom of the NMR tube. Repeated ^{31}P NMR spectra only showed the resonance of the $Ag(P_4)_2^+$ cation but not that of free P_4 or binary phosphorus sulfides.[15b] Therefore we concluded that the reaction according to Equation (5) is certainly endergonic.

[33] B. C. Guo, A. W. Castleman, *Chem. Phys. Lett.* **1991**, *181*, 16.

[34] In detail: $\Delta_f H^{298}$ ($[Ag(S_8)_2]^+$, g) = $\Delta_f H^{298}$ (Ag^+, g) + $2\Delta_f H^{298}$ (S_8, g) – $\Delta_r H^{298}$ (Eq. a), $\Delta_f H^{298}$ ($[Ag(S_8)_2]^+$, g) = 1017 + 2 × 101 – 363 = 856 kJ mol^{-1}. $\Delta_f H^{298}([AgS_8]^+$, g) = $\Delta_f H^{298}(Ag^+$, g) + $\Delta_f H^{298}(S_8$, g) – $\Delta_r H^{298}$(Eq. b), $\Delta_f H^{298}([AgS_8]^+$, g) = 1017 + 101 – 212 = 902 kJ mol^{-1}.

[35] Only HF orbital energies give the correct energetic leveling of the orbitals, however, they always lead to too-large HOMO–LUMO gaps. The inclusion of electron correlation reduces the HOMO–LUMO gap and would further reduce the energetic separation of the S_8 HOMO and the Ag^+ LUMO. However, if electron correlation is treated by DFT, which is known to give a very unreliable energetic leveling of the orbitals, the calculation leads to the inverse situation (i.e., the energy of the S_8 HOMO is calculated at –0.240 a.u.—*higher* in energy than the Ag^+ LUMO at –0.419 a.u. (BP86/TZVPP); cf. HF values in text). With perturbation theory MP2 intrinsically no clear orbital energies can be assigned and, therefore, we state the HF/TZVPP values here and suggest that the inclusion of electron correlation gives a smaller energetic separation of the S_8 HOMO and the Ag^+ LUMO; this leads to a more favorable interaction.

[36] At 200 K the thermal energy is higher than the small bond energy of the weak S–F contacts. Therefore the displacement parameters of the CF_3 groups are large; this indicates almost free rotation around the C–C bond and no distortion of the cation. However, upon cooling to 150 K, the thermal energy available is reduced and now the weak bond energy of the S–F contacts is large enough to hinder the free rotation of the CF_3 groups around the C–C bond and distort the $[Ag(S_8)_2]^+$ geometry (cf. the shallow PES of the $Ag(S_8)_2^+$ cation found in the computation). Consequently the thermal ellipsoids of the CF_3 groups are much smaller in the 150 K determination (see ellipsoid plot in the Supporting Information). In agreement with the quantum-chemical calculations above, it is also concluded that the energetic difference between the geometry of the $[Ag(S_8)_2]^+$ cation in **3** at 150 K) and at 200 K is very small (cf. the difference in thermal energy of $\frac{3}{2}R\Delta T$ amounts to only 0.6 kJ mol^{-1}, $\Delta T = 200 - 150$ K = 50 K).

[37] W. Koch, M. C. Holthausen, *A Chemists Guide to Density Functional Theory*, Wiley-VCH, Weinheim, **2000**.

[38] F. Jensen, *Introduction to Computational Chemistry*, **1999**, Wiley, New York.

[39] For comparison: The optimization of C_i $[Ag(S_8)_2]^+$ at the (RI-)MP2/TZVPP level took 21 days on a parallel version of the program TURBOMOLE with two 700 MHz Athlon processors with 512 MB of RAM each! No (RI-)MPn ($n > 2$) method has yet been implemented. Since the RI approximation makes an RI-MP2 calculation versus a conventional MP2 calculation faster by a factor of 10 it is still impossible to use higher correlated methods such as MP3, MP4 or, even more expensive, CCSD(T).

[40] From the literature it is clear that the effect of $(n+1)$p orbital contributions on the geometry of *strongly bound* systems is relatively small (0.01–0.02 Å)[40d] and the energetic stabilization of a given bond due to $(n+1)$p metal–ligand interactions is smaller than that of the primary interaction. A suitable example to illustrate this is the bond lengths and bond energy of the four Ni–CO bonds in $Ni(CO)_4$, which are elongated by about 0.01 Å and destabilized by 66 kJ mol^{-1} (or 15% of the total binding energy) when the 4p basis set on Ni is excluded from the calculation.[40d] However, in the $[Ag(S_8)_2]^+$ cation a series of *weak interactions* has to be accounted for. Weak bonds reside in a shallow potential where small energetic changes may lead to strong changes in the bond length. Therefore we include the presumably weak bonding contributions of the empty silver $5p^0$ acceptor orbitals in our discussion. Key references are: a) C. R. Landis, T. K. Firman, D. M. Root, T. Cleveland, *J. Am. Chem. Soc.* **1998**, *120*, 1842; b) C. A. Bayse, M. B. Hall, *J. Am. Chem. Soc.* **1999**, *121*, 1348; c) D. Axel, F. M. Bickelhaupt, G. Frenking, *J. Am. Chem. Soc.* **2000**, *122*, 6449; d) P.-D. Fan, P. Deglmann, R. Ahlrichs, *Chem. Eur. J.* **2002**, *8*, 1059.

[41] a) A. J. Lupinetti, V. Jonas, W. Thiel, S. H. Strauss, G. Frenking, *Chem. Eur. J.* **1999**, *5*, 2573; b) C. W. Bauschlicher, Jr., S. R. Langhoff, H. Partridge, *J. Chem. Phys.* **1991**, *94*, 2068; c) J. D. Dunitz, L. E. Orgel, *Adv. Iorg. Chem. Radiochem.* **1960**, *2*, 1; d) This was attributed to the costly rehybridization of the metal M (to sd) which has to be paid by the first ligand L so that the bond energy of the second ligand L to give ML_2^+ is then fully released, see [41a-c].

[42] The preferential linear arrangement of many linear d^{10} coinage-metal systems[41a-c] is induced by an sd hybridization of one (occupied) 4d orbital and the empty 5s orbital; this leads to an occupied and an empty sd hybrid orbital shown in Figure 12.
The shortest Ag–S bonds in $[Ag(S_8)_2]^+$ of 2.68–2.71 Å are *trans* to one another and probably due to an interaction of the occupied sulfur $3p^2$ lone-pair donor–donor orbitals with the empty silver sd-hybrid acceptor orbital as shown in Figure 13b. The longest Ag–S lengths

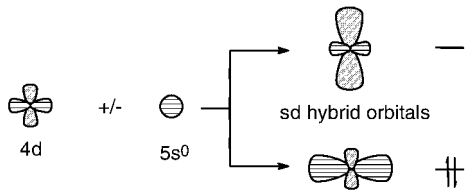

Figure 12. sd-hybrid-orbital formation leading to linear d^{10} coinage-metal complexes.

in $[Ag(S_8)_2]^+$ of 3.31 – 3.35 Å are orthogonal to the shortest Ag–S bonds. The occupied silver sd hybrid orbital must be found orthogonal to the empty sd silver hybrid orbital. A repulsive linear arrangement of three occupied orbitals, as in Figure 13a, results and leads to the observed longest Ag–S separation. However, the remaining four intermediate Ag–S separations at 2.92 – 3.20 Å (Figure 3) cannot be explained by an interaction as in Figure 13. Moreover, it was shown that in sd hybridized $[ML_2]^+$ systems (M = coinage metal) the dissociation enthalpy of the first ligand L is higher than that of the second ligand L, that is, ΔH for $[ML_2]^+ \rightarrow ML^+ + L$ is higher than $ML^+ \rightarrow M^+ + L$.[41d] In our $[Ag(S_8)_2]^+$ case, all levels agree that the dissociation of the first S_8 molecule is easier to achieve than that of the second (cf. Table 7). Therefore and due to the, in total, *eight* Ag–S contacts below the sum of the Ag and S van der Waals radii of 3.50 Å an alternative—and to our belief better—bonding model that does not require the unusual polarization of the closed $4d^{10}$ silver shell was proposed (see main text).

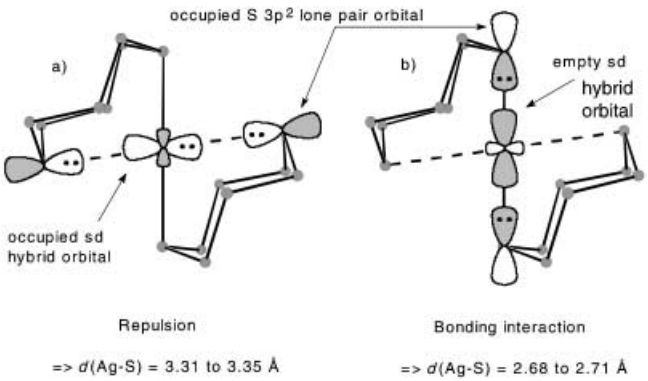

Figure 13. a) Repulsive linear arrangement of two occupied sulfur $3p^2$ lone-pair orbitals and one occupied silver sd hybrid orbital. b) Bonding interaction of two occupied sulfur $3p^2$ lone-pair orbitals and one empty silver sd hybrid orbital.

[43] When the silver ion approaches the S_8 molecule, two different bonding modes between the occupied sulfur $3p^2$ lone-pair donor orbitals in the 1,3-position and the two empty orthogonal silver $5p^0$ acceptor orbitals are possible: i) a symmetric combination forming two equal Ag–S bonds giving, in total, a planar tetracoordinate primary coordination environment of the silver ion (local AgS_4 symmetry is D_{2h}). ii) a less symmetric combination leading to one strong and one weak interaction giving, in total and to a first order of approximation, linear dicoordination and a second set of weaker Ag–S bonds that complete the Ag coordination environment to planar as in the experiment (local AgS_4 symmetry is C_{2h}). Since two p orbitals are at an angle of 90°, the ideal S-Ag-S bond angle for (i) would be 90° (1,3 coordination). When (ii) is correct, the cation can accommodate much sharper S-Ag-S bond angles (cf. the experimental S-Ag-S bond angles in **3** (200 K) and **4** are 70.3°). The $\{AgS_8\}$ moiety of the solid-state structure of **1** provides a coordination geometry as in (i) with two almost equal Ag–S interactions at 2.744 and 2.792 Å. Here the S-Ag-S bond angle is 72.0° and still considerably smaller than the ideal 90° value needed for (i). This shows that, due to geometric restrictions, an optimal orbital overlap for a bonding as in (i) is impossible, and when cation – anion interaction is minimized in going from **1** to **3**/**4** the $Ag(S_8)_2^+$ cation therefore interact as in (ii).

[44] a) C. A. Coulson, *J. Chem. Soc.* **1964**, 1442; b) J. G. Malm, H. Selig, J. Jortner, S. A. Rice, *Chem. Rev.* **1965**, *65*, 199.

[45] Compare: fourfold symmetry of the S_8 ring and threefold symmetry of the $5p^0$ orbitals in this orientation. Therefore it is geometrically impossible for the axial Ag $5p^0$ orbital (see Figure 9) to strongly interact with the remaining four S $3p^2$ lone-pair orbitals above and below the central plane.

[46] a) T. S. Cameron, H. K. Roobottom, I. Dionne, J. Passmore, H. D. B. Jenkins, *Inorg. Chem.* **2000**, *39*, 5614; b) I. Krossing, J. Passmore, *Inorg. Chem.* **1999**, *38*, 5203.

[47] Moreover the arrangement in D_{4d} S_8 was shown to be determined by electrostatic repulsion of the occupied $3p^2$ lone-pair orbitals; therefore, adjacent $3p^2$ lone-pair orbitals are orthogonal, and the S-S-S-S torsion angles are close to 90°.[48] Although electron density is removed from the $3p^2$ lone-pair orbitals through the Ag^+ coordination, and weak π bonding could therefore occur, the orthogonal orientation of the $3p^2$ lone-pair orbitals precludes $3p_\pi - 3p_\pi$ bonding.

[48] a) R. Steudel, *Top. Curr. Chem.* **1981**, *102*, 149; b) Y. Drozdova, R. Steudel, *Phosphorus, Sulfur, Silicon Relat. Elem.* **1997**, *124/125*, 521.

[49] a) N. Bartlett, D. H. Lohmann, *J. Chem. Soc.* **1962**, 5253; b) N. Bartlett, D. H. Lohmann, *Proc. Chem. Soc. London* **1962**, 115.

[50] N. Bartlett, *Proc. Chem. Soc. London* **1962**, 218.

[51] T. Drews, K. Seppelt, *Angew. Chem.* **1997**, *109*, 264; *Angew. Chem. Int. Ed. Engl.* **1997**, *36*, 273.

[52] C. A. Reed, K.-C. Kim, R. D. Bolskar, L. J. Mueller, *Science* **2000**, *289*, 101.

[53] a) D. D. Wagman, W. H. Evans, V. B. Parker, R. H. Schumm, I. Halow, S. M. Bailey, K. L. Churney, R. L. Nuttal, *J. Phys. Chem. Ref. Data*, **1982**, *11*, Suppl. 2; b) S. G. Lias, J. E. Bartmess, J. F. Liebman, J. L. Holmes, R. D. Levin, W. G. Mallard, *J. Phys. Chem. Ref. Data*, **1988**, *17*, Suppl. 1; c) *CRC Handbook of Chemistry and Physics* (Ed.: D. R. Lide), CRC Press, Boca Raton; d) http://www.nist.gov/chemistry.

[54] There is a roughly linear dependence between the sublimation enthalpy of a nonpolar molecule (no H bridges) and its atomic weight, and therefore heavy molecules are also expected to have higher sublimation enthalpies. This is shown by the following series of experimental sublimation enthalpies (in kJ mol^{-1}): OsO_4 ($M_r = 254$, $\Delta H_{subl} = 57$), $TiBr_4$ ($M_r = 367$, $\Delta H_{subl} = 67$), WCl_6 ($M_r = 367$, $\Delta H_{subl} = 89$), Nb_2Cl_{10} ($M_r = 540$, $\Delta H_{subl} = 94$), TiI_4 ($M_r = 555$, $\Delta H_{subl} = 98$), C_{60} ($M_r = 721$, $\Delta H_{subl} = 175$), and C_{70} ($M_r = 841$, $\Delta H_{subl} = 200$). The linear dependence is shown in a deposited figure.

[55] a) I. Krossing, I. Raabe, *Angew. Chem.* **2001**, *113*, 4544; *Angew. Chem. Int. Ed.* **2001**, *40*, 4406; b) I. Krossing, *J. Chem Soc. Dalton Trans.* **2002**, 500.

[56] A. Decken, I. Krossing, J. Passmore, F. Steden, unpublished results.

[57] I. Krossing, J. Passmore, unpublished results.

[58] The $[Al(pftb)_4]^-$ anion is water and HNO_3 (35 weight %) stable (Cs, Li, Ag salts).

[59] M. P. Murchie, R.Kapoor, J. Passmore, G. Schatte, *Inorg. Synth.* **1996**, *331*, 80.

[60] The $Ag[Sb(OTeF_5)_6]$ used in this experiment was prepared from $AgOTeF_5$ (18.0 mmol, 6.25 g) and $SbCl_5$ (3.51 mmol, 2.65 mL of a 1.326 M stock solution in F-114) in F-114 (22.84 g). CH_2Cl_2 (12 – 15 mL) was added to extract the $Ag[Sb(OTeF_5)_6]$. The soluble material was subjected to a dynamic vacuum for 12 h and isolated (4.632 g). In the ^{19}F NMR (CH_2Cl_2) of this soluble material only lines attributable to $Ag[Sb(OTeF_5)_6]$ were observed.

[61] Direct connection: A 6.35 mm glass tube incorporating one valve to allow flame drying. The reaction vessels were connected to the direct connection by Gyro Lock fittings (Swage Lock Corp.). A short (2 cm) Teflon tube was inserted into the glass tube within the Gyro Lock to avoid contact between metal and solution.

[62] SAINT 6.02, **1997 – 1999**, Bruker AXS, Inc., Madison, Wisconsin, USA.

[63] SADABS George Sheldrick, **1999**, Bruker AXS, Inc., Madison, Wisconsin, USA.

[64] SHELXTL 5.1, George Sheldrick, **1997**, Bruker AXS, Inc., Madison, Wisconsin, USA.

  0947-6539/02/0815-3400 $ 20.00+.50/0 *Chem. Eur. J.* **2002**, *8*, No. 15

[65] A. Apbett, F. Grein, J. P. Johnson, J. Passmore, P. S. White, *Inorg. Synth.* **1986**, *25*, 422.
[66] N. Walker, D. Stuart, *Acta.Crystallogr.* **1983**, *A39*, 158.
[67] TEXSAN–TEXRAY Single-Crystal Structure-Analysis Package, Version 5.0, Molecular Structure Corporation, The Woodlands, Texas, **1989**.
[68] TURBOMOLE, Version 5: a) R. Ahlrichs, M. Bär, M. Häser, H. Horn, C. Kölmel, *Chem. Phys. Lett.* **1989**, *162*, 165; b) M. v. Arnim, R. Ahlrichs, *J. Chem. Phys.* **1999**, *111*, 9183; c) O. Treutler, R. Ahlrichs, *J. Chem. Phys.* **1995**, *102*, 346; d) current version: http://www.chemie.uni-karlsruhe.de/PC/TheoChem.
[69] a) K. Eichkorn, F. Weigend, M. Häser, R. Ahlrichs, *Theor. Chim. Acta* **1997**, *97*, 331; b) K. Eichkorn, O. Treutler, H. Ohm, M. Häser, R. Ahlrichs, *Chem. Phys. Lett.* **1995**, *242*, 652.
[70] a) J. P. Perdew, *Phys. Rev. B* **1986**, *33*, 8822; b) A. D. Becke, *Phys. Rev. A* **1988**, *38*, 3098; c) S. H. Vosko, L. Wilk, M. Nusair, *J. Can. Phys.* **1980**, *58*, 1200.
[71] a) A. Schäfer, H. Horn, R. Ahlrichs, *J. Chem. Phys.* **1992**, *97*, 2571; b) A. Schäfer, C. Huber, R. Ahlrichs, *J. Chem. Phys.* **1994**, *100*, 5829.
[72] D. Andrae, U. Haeussermann, M. Dolg, H. Stoll, H. Preuss, *Theor. Chim. Acta* **1990**, *77*, 123.
[73] A. Klamt, G. Schürmann, *J. Chem. Soc. Perkin. Trans.* **1993**, *2*, 799.
[74] Thermal and entropic contributions to the enthalpy and free energy were obtained by fully optimizing all the species in question with Gaussian98W[75] at the simple HF/LANL1MB level. All species also represented true minima without imaginary frequencies at the HF/LANL1MB level. ZPEs were taken from the BP86/SVP calculation. Since statistic thermodynamics is little influenced by the employed geometries, and the entropic contributions mainly arise from the moment of inertia of a species, it is believed that errors associated with this procedure are very small if it used consistently.
[75] *Gaussian 98* (Revision A.3), M. J. Frisch, G. W. Trucks, H. B. Schlegel, G. E. Scuseria, M. A. Robb, J. R. Cheeseman, V. G. Zakrzewski, J. A. Montgomery, R. E. Stratmann, J. C. Burant, S. Dapprich, J. M. Millam, A. D. Daniels, K. N. Kudin, M. C. Strain, O. Farkas, J. Tomasi, V. Barone, M. Cossi, R. Cammi, B. Mennucci, C. Pomelli, C. Adamo, S. Clifford, J. Ochterski, G. A. Petersson, P. Y. Ayala, Q. Cui, K. Morokuma, D. K. Malick, A. D. Rabuck, K. Raghavachari, J. B. Foresman, J. Cioslowski, J. V. Ortiz, B. B. Stefanov, G. Liu, A. Liashenko, P. Piskorz, I. Komaromi, R. Gomperts, R. L. Martin, D. J. Fox, T. Keith, M. A. Al-Laham, C. Y. Peng, A. Nanayakkara, C. Gonzalez, M. Challacombe, P. M. W. Gill, B. G. Johnson, W. Chen, M. W. Wong, J. L. Andres, M. Head-Gordon, E. S. Replogle, J. A. Pople, Gaussian, Inc., Pittsburgh PA, **1998**.

Received: January 17, 2002 [F3807]